LAND SUBSIDENCE MODELING USING SPACEBORNE GEODETIC TECHNIQUES AND FIELD BASED MEASUREMENTS

Thesis submitted to the Andhra University, Visakhapatnam in partial fulfilment of the requirement for the award of *Master of Technology in Remote Sensing and GIS*

Submitted By:
Sumi Kala
M.Tech Remote Sensing & GIS
(Specialization in Geosciences)

Supervised By:
Dr. R.S.Chattejee
Scientist 'SG', GSGHD

Indian Institute of Remote Sensing, ISRO,
Dept. of Space, Govt. of India Dehradun – 248001
Uttarakhand, India

Aug, 2015

LAND SUBSIDENCE MODELING USING SPACEBORNE GEODETIC TECHNIQUES AND FIELD BASED MEASUREMENTS

Thesis submitted to the Andhra University, Visakhapatnam in partial fulfilment of the requirement for the award of *Master of Technology in Remote Sensing and GIS*

Submitted By:
Sumi Kala
M.Tech Remote & GIS
(Specialization in Geosciences)

Supervised By:
Dr. R.S.Chattejee
Scientist 'SG', GSGHD

Indian Institute of Remote Sensing, ISRO,
Dept. of Space, Govt. of India Dehradun – 248001
Uttarakhand, India

Aug, 2015

DISCLAIMER

This work has been carried out in partial fulfilment of Masters in Technology program in Remote Sensing and Geographic Information System at Indian Institute of Remote Sensing, Dehradun, India. The author is solely responsible for the contents of the thesis.

Date: 16 June, 2015 **Sumi Kala**

CERTIFICATE

This is to certify that the project entitled **Land Subsidence Modelling Using Spaceborne Geodetic Techniques and Field Based Measurements”** is a bona fide record of work carried out by **Ms. Sumi Kala**. The report has been submitted in partial fulfilment of requirement for the award of Master of Technology in Remote Sensing and GIS in Natural Resource Management with specialization in Geosciences, conducted at Indian Institute of Remote Sensing (ISRO), Dehradun from 19 Aug 2014 to 14 Aug 2015. The work has been carried out under the supervision of **Dr. R. S. Chatterjee**, Scientist / Engineer ‘SG’, Geosciences and Geohazards Department.

No part of this report is to be published without the prior permission/intimation from/to the undersigned.

Dr. P. K. Champati ray
Group Head, G&DMS
IIRS, Dehradun

Dr. R.S. Chatterjee
Scientist/Engineer ‘SG’,
Faculty, G&DMS
IIRS, Dehradun

Dr. A Senthil Kumar
Director
IIRS, Dehradun

Dr. S.P.S. Kushwaha
Dean (Academics) &
Group Director, ERSSG
IIRS, Dehradun

Acknowledgement

I owe my gratitude to all those people who have made this dissertation possible. First and foremost, I would like to thank my supervisor, Dr. R.S.Chatterjee for his continuous support, patience, motivation, enthusiasm and immense knowledge. His guidance helped me throughout the research work and writing of this thesis.

A very special thanks to Ashutosh Bharadwaj, who helped me a lot in carrying out DGPS survey. His extensive experience in carrying out surveys helped me gain immense knowledge and made me capable enough to carry out the surveys independently.

I wish to express my deepest gratitude to my Dr. P.K. Champati Ray, Head GSGHD for his constant encouragement, insightful comments and feedback.

I would like to thank Dr. Y. V. N. Krishnamurthy (former Director, IIRS) and Dr. Senthil Kumar (Director, IIRS) for providing the support and infrastructure needed for the implementation of this project.

I thank Shailja Thapa for her patient support during this research work. Also, a special thanks to Ashish Dhiman for his continuous technical support.

My heartfelt thanks to my friends and fellow mates, Rohit, Shobhana, Utsav, Narendra, Sudarshan, Bipin, Chayanika, Somalin and Aniket for always being there me.

I would also like to express my gratitude to the officials and other staff members of Indian Institute of Remote Sensing, who provided their help during the period of my project work.

Sumi Kala

Abstract

Groundwater level in North-western states of India is declining severely. Drawdown leads to subsidence which may cause permanent compaction of the aquifers and may also cause damage to buildings. In this study Differential Interferometric SAR technique (DInSAR) has been used to identify and measure the rate of deformation in Delhi and Chandigarh and its surroundings. DInSAR provides wide spatial coverage which helps in mapping the spatial extent of the subsidence area. High Resolution CARTOSAT DEM ensures that the fringes are not due to DEM error. Deformation phase in each fringe was calculated from the unwrapped differential interferogram by phase profiling technique. Predictive Modelling helps to estimate the future land subsidence scenario under the influence of declining piezometric head of the aquifer system. Both Delhi and Chandigarh areas are mainly covered with alluvium. Clay, mixed with sand and silt, with thickness of more than 40 meters is present in parts of Delhi. Inelastic compaction of the confining layers and elastic compaction of the aquifers were calculated individually for several piezometric wells, distributed in entire Delhi. Differential Interferograms show that Palam area near Dwarka in Delhi, Kapashera in Gurgaon, and Mohali, Kharar, Banur in Chandigarh and surrounding areas are undergoing deformation. The fringes are coinciding with the highly built up areas. ALOS L-Band, FBS data, in Dwarka, Gurgaon shows an avergae deformation rate of 5.69cm/year and 5.89 cm/year respectively during 2009 -2011. In Delhi, Radarsat -2 C Band data also shows average deformation rate of 4.56 cm/year during 2013-2015. Predictive modeling over Delhi shows potential deformation of 4.48 cm/year and 2.14 cm/year for Dwarka and Gurgaon respectively during 2008-2011. The results of predictive modeling show higher values correspond to DInSAR which points to a relationship between subsidence and groundwater depletion.

Keywords: *DInSAR, Predictive Modelling, groundwater, depletion, subsidence*

Table of Contents

List of Figures

List of Tables

1. Introduction

1.1 Background

Land subsidence, is the sinking of the Earth's surface due to movement of the subsurface materials. It may be sudden process if associated with tectonic activity however, groundwater induced subsidence is a gradual sinking of the Earth's surface. Land Subsidence induced by excessive withdrawal of groundwater, has been witnessed in several parts of the world, including Las Vegas (Amelung et al., 1999), California (Galloway et al., 1998),Iran (Motagh et al., 2006), Kolkata (Chatterjee et al., 2006) and many others. Excessive pumping of groundwater leads to over-exploitation of the aquifers which is a problem of serious concern. Land Subsidence, thus caused is due to compaction of the aquifer system (Galloway, et al., 1998). The rate of Land Subsidence may vary from few millimeters as observed in Turkey (and others) up to few meters as in case of Mexico, California and Arizona (Sahu and Sikdar, 2011).

Groundwater is the major source of fresh water in not only India but also in other parts of the world. Groundwater depletion is one of the major problems affecting North West India. According to the study carried out using GRACE data, the mean ground water depletion rate was estimated to be about 4 ± 1.0 cm yr-1 over the north-western Indian states of Rajasthan, Punjab and Haryana (Rodell et al., 2009). Over a period of time, Delhi has experienced an exponential growth of its population (Census, 2011). This has caused increased reliance of domestic water supply on groundwater supply from aquifers. Groundwater level data of May 2011 in comparison with 10 year mean of May water level, it shows that 40% of wells show a fall in the range of 0.02 to 14.07 m. The maximum fall has taken place in South-West, North-West and North districts i.e. 9.76 to 14.07 m (Groundwater Year Book, 2011-2012). This has led to aquifer system overdraft, as the rate of pumping exceeds the rate of recharge.

Aquifer System Compaction is the deformation of the aquifer system that cannot be recovered indicating a permanent loss of aquifer system storage. Even though Land Subsidence causes considerable damage to manmade structures including buildings, railways, bridges, etc., yet it remains one of the least studied adverse impact of groundwater development. For confined aquifers, water is mainly stored in the porous material constituting the aquifer. In such cases, when the pore fluid reduces to an extent such that it caused an increase in the effective stress to values greater than past maximum effective stress, the fine grained aquitards undergo compaction (Galloway et al., 1998). The compaction of the aquitards in inelastic and cannot be recovered. Compressibility of the aquifer system determines the storage capacity (Hoffman, 2003).

Even though Field based Measurements provide very accurate results, it is very difficult and expensive to measure the compaction at several locations. Therefore, in order to identify the critical areas Differential Interferometric SAR (DInSAR) technique has been used. InSAR has been extensively used in different parts of the world over the years for Land Subsidence Mapping and Monitoring. It was first used by Galloway and others in 1998 for detecting Land Subsidence cause due to aquifer system compaction. Followed by several others Amelung et al., 1999, Strozzi et al., 2001, Motagh et al., 2006, Chatterjee, et al., 2006, Hung et al., 2010 and several others have shown the use of Interferometric Technique. In this study I have focused on the application of DInSAR for detecting, monitoring and interpreting land subsidence caused by aquifer system deformation.

Interferometry is based on the principle of phase difference of two images acquired from same viewing angle but at different times. DInSAR Interferogram is a product of two SAR mages acquired at different times with topographic phase removed using a Digital Elevation Model (DEM). Phase Difference gives information about path difference of two signal which can be measured with subwavelength accuracy (Galloway et al., 1998). The best characteristics of InSAR is that it provides extensive spatial coverage at very high resolution. Thus it makes possible to quantify the regional extent of subsidence (Ding, et al., 2004). Low wavelength (C-Band) as well as high wavelength (L-Band) SAR data has the capability to measure slow and rapid subsidence at millimeter level of accuracy. In this study both ALOS (L-Band) and RADARSAT-2 (C-Band) data has been used. The disadvantage of DInSAR is that it may be affected by several errors thus reducing its accuracy (Hung, et al., 2010). The important sources of error are the spatial and the temporal baseline de-correlation. Higher is the baseline, more is the de-correlation. To avoid these errors, interferometric pairs which do not exceed the critical limit and maintain high coherence are used. Therefore, coherence between the master and slave images plays a vital role in deciding the quality of the interferogram. The land subsidence measurement rates are determined from the phase unwrapped image. Profiling across the fringe areas is done to determine the phase difference that gives the path difference and finally the rate.

Land Subsidence is a consequence of Aquifer System Compaction, which may vary in extent over different seasons i.e. pre-monsoon and post-monsoon depending upon the groundwater level decline (Amelung et al., 1999). Predictive Modelling of the aquifer system compaction is done depending upon the lowering of groundwater level. This helps in modelling the elastic compaction of the aquifer and inelastic compaction of the aquitards. Several parameters like thickness of the aquifer, thickness of confining layers, porosity of the aquifer and several other parameters were taken into account. Cumulative compaction is calculated over the years and spatially interpolate to get the overall scenario in Delhi. The rate of subsidence depends upon the underlying subsurface soil properties of fine grained silt and clay compacts more in comparison to coarse gained sand and gravel (Ganguli, 2011). Considering the present scenario, the rate at which groundwater is depleting, it is very important to predict the future scenario of Land Subsidence.

GPS determines the three dimensional point positions i.e. two in horizontal direction and one in vertical direction which can be helpful for measuring the Land Subsidence. For a long, GPS static surveys technique has been quite intensively used for studying and monitoring land subsidence. Several successful studies have been done using GPS in different parts of the world like in Indonesia (Abidin et al., 2008), Bandung (Chatterjee et al., 2013), Taiwan (Hung et al., 2010), Iran (Motagh et al., 2006) and several others.

Field based measurements, using Extensometer gives the actual measurement of compaction of the confining layers and the aquifer. Extensometer measures the compaction of the aquifer system at different depths and is the best technique to understand the mechanism of subsidence (Hung et al., 2010). Vibrating Wire Borehole Extensometer consists of protective tubes, anchors, rods and VW displacement sensors. The VW transducer measures settlement or heaving and changes frequency signal as movement in layers change. Though it provides discrete information, however it has high accuracy (about 1-5mm) and stability. Since it is expensive to use extensometer at several locations, they remain limited to the core areas of subsidence as identified by DInSAR.

1.2 Problem Statement and Motivation

Groundwater in India is a critical natural resource. Even then, an increasing number of aquifers are reaching unsustainable levels of exploitation. If current trend continues, in 20 years about 60% of all India's aquifers will be in a critical condition says a World Bank report, Deep Wells and Prudence. More than 60% of irrigated agriculture and 85% of drinking water supplies are dependent on groundwater. Urban population increasingly depend on groundwater due to unreliable and inadequate municipal water supplies.

As per the Central Ground Water Board, 2012-13 report the Annual Replenishable Ground Water Resource for the entire country is 431 billion cubic meter (bcm), Net Annual Ground Water availability is 396 billion cubic meter whereas the annual ground water draft for irrigation, domestic and Industrial is 243 billion cubic meter. If groundwater resources continue to be exploited at similar rates, it would not take long for the resources to diminish completely.

The population of Delhi has increased from 1.28 crores to 1.67 crores (Census, 2011) registering an increase of over 21 per cent during the period of 2001-2011. Seven out of nine districts of Delhi are categorized as overexploited with respect to dynamic groundwater resources. Even though the groundwater resources are over exploited, hardly drinking water supply can be met. Therefore, overdraft of groundwater can be one of the major reasons causing aquifer system compaction. In Punjab 80% well are overexploited out of which 2 % are critical. 76% of the wells have shown fall in water level since 2003. Delhi and Chandigarh surroundings are mostly covered by alluvial sediments which make them more prone to Land Subsidence.

DInSAR is one of the promising remote sensing technology for subsidence monitoring, which combines synthetic radar imaging theory and electromagnetic wave interferometric technology. DInSAR technique can provide data in varied weather condition, spatially continuous and high spatial resolution, so the cost is relatively lower than conventional methods. GPS provides discrete information however; it is accurate enough to validate DINSAR results. Extensometer ensures whether subsidence observed is associated with groundwater depletion or not. Therefore, in this study, an attempt has been to accurately map the areas undergoing Land

1.3 Research Objectives

- Space-borne geodetic observations such as DInSAR for mapping, measurement and modelling of Land Subsidence in Delhi and Chandigarh.
- Field based observation by vibrating wire Piezometer and Extensometer to assess aquifer system compaction due to groundwater depletion.
- Comparison of space-borne geodetic and ground based observations.
- Potential land subsidence scenario identification by predictive modelling of aquifer system compaction.

1.4 Research Questions

- How effectively can DInSAR help in measurement and modelling of land subsidence and how can the measurement rates be improved?
- How far layer compression is taking place due to groundwater depletion?
- How close are the space-borne geodetic and ground based observations?
- How far groundwater level decline is correlated with land subsidence and can further help in predicting subsidence potential areas?

2. Literature Review

2.1 Land Subsidence

Land Subsidence is settlement of the ground surface that may be because of natural or anthropogenic causes. It may occur suddenly due to tectonic deformation, sinkhole or underground mine collapse. Whereas, it can take place slowly, becoming evident after a long span of time as in case of aquifer system compaction due to excessive withdrawal of groundwater (Whittaker, 1989). In this study I have focused on aquifer system compaction process because, depletion of groundwater has been witnessed in the study area. The spatial extent and shape of the surface displacements observed in this work strongly suggests that deformation process is due to pumping from the groundwater reservoir (Hoffman, 2003). A brief explanation has been given below for neglecting other factors.

Compaction due to Construction:
The interferometric phase difference is only meaningful where the signals in the two SAR acquisitions remain coherent. Construction, ploughing, or significant erosion destroy this coherence by altering the geometry of the surface at the scale of the radar wavelength. Thus it can lead to errors or prevent any measurement of the surface displacement, but they cannot bias the displacement measurement.

Tectonic deformation:
Tectonic processes can cause dramatic surface displacements. During, these years, no major tectonic event has happened. Even more, the patterns of tectonic surface deformation are typically highly suggestive of the process underlying. If any deformation related to these faults occur, it would affect the area broadly or be discontinuous across the fault.

Oil & Gas Extraction and Mining
No Oil Gas reservoirs and underground mines exist under the areas studied here and therefore need not be considered.

2.2 Aquifer System Compaction

2.2.1 Aquifer

Aquifer is a geological unit that can store and transmit water at sufficient rate to supply out to wells. Confining layer is a geological unit that can store but it cannot transmit water because of its low permeability, such as clay. Unconfined aquifers are those with no confining layer above whereas those with confining layers above are called confined aquifers.

2.2.2 Hydraulic Head and Effective Stress

Hydraulic head or the piezometric head is the height to which the water the water will rise in a bore in confined aquifer. The changes in Hydraulic head (h) are directly proportional to the changes in pore pressure given by the following equation:

$$h = h_z + \frac{p}{\rho g} = h_z + \frac{p}{\gamma w} \tag{2.1}$$

Where, h_z is called the elevation head, the distance to an arbitrary reference surface, $\gamma w = \rho g$ is the specific weight (specific gravity) of water and p is the pore pressure. At a known point, the hydraulic head reflects the sum total of energy of water in porous medium (Rooij, et al., 2009).

The pressure transmitted through grain to grain contact is termed as intergrannular or effective pressure. This effective pressure is responsible for decrease in the void ratio of a soil mass. This pressure is called as pore pressure i.e. pressure exerted by the water present in the pores of soil mass. The overburden weight which includes rock and water creates a downward stress σ_T on a saturated aquifer. This stress is bared by the porous aquifer and the fluid pressure p of the water in the pore spaces. Terzaghi was the first to explicitly explain this concept of effective stress in relation to the consolidation of clays. Terzaghi's principle of effective stress, in relation to aquifer compaction has been explained by several authors (Galloway et al., 1998; Galloway et al., 2013; Hoffman, 2003; Hung et al., 2012; Murthy, 2002). The total Stress, σ_T, on the confined aquifer system is equal to the sum of the pore pressure, p, and the effective stress (σ_e) given by:

$$\sigma_T = \sigma_e + p \tag{2.2}$$

$$d\sigma_T = d\sigma_e + dp \tag{2.3}$$

Where, $d\sigma_T$ is the change in the total stress, $d\sigma_e$ is the change in effective stress, dp is the change in fluid pressure. In a saturated porous medium, the overburden weight remains same over a period of time. In such cases, the change in the total stress $d\sigma_T = 0$, and

$$d\sigma e = -dp \tag{2.4}$$

This equation states effective fluid pressure and effective stress are inversely proportion i.e. if the fluid pressure increases, the effective stress decreases by an equal amount; and if the fluid pressure decreases, the effective stress increases by an equal amount. Fluid pressure can be expresses in terms of hydraulic head as:

$$p = \rho g h = \rho g\ (h - z) \tag{2.5}$$

Differentiating equation 2.5 gives:

$$\mathrm{dp} = \rho \mathrm{gdhp} = \rho \mathrm{h}(\mathrm{h} - \mathrm{z}) = \rho \mathrm{gdh} \tag{2.6}$$

Substituting this in equation 2.4 above gives:

$$\mathrm{d}\sigma\mathrm{e} = - \rho \mathrm{gdh} \tag{2.7}$$

Thus it states that the change in effective stress $d\sigma_e$ at a given point in saturated aquifer is governed by the change in the hydraulic head at that point.

2.2.3 Aquifer System Deformation

Effective stress increases as pressure head is reduced due to pumping of groundwater. This increasing stress leads to compaction of over drafted aquifer systems occurs as a result of consolidation of aquitards i.e. compressible clay and silt deposits, in the aquifer system.

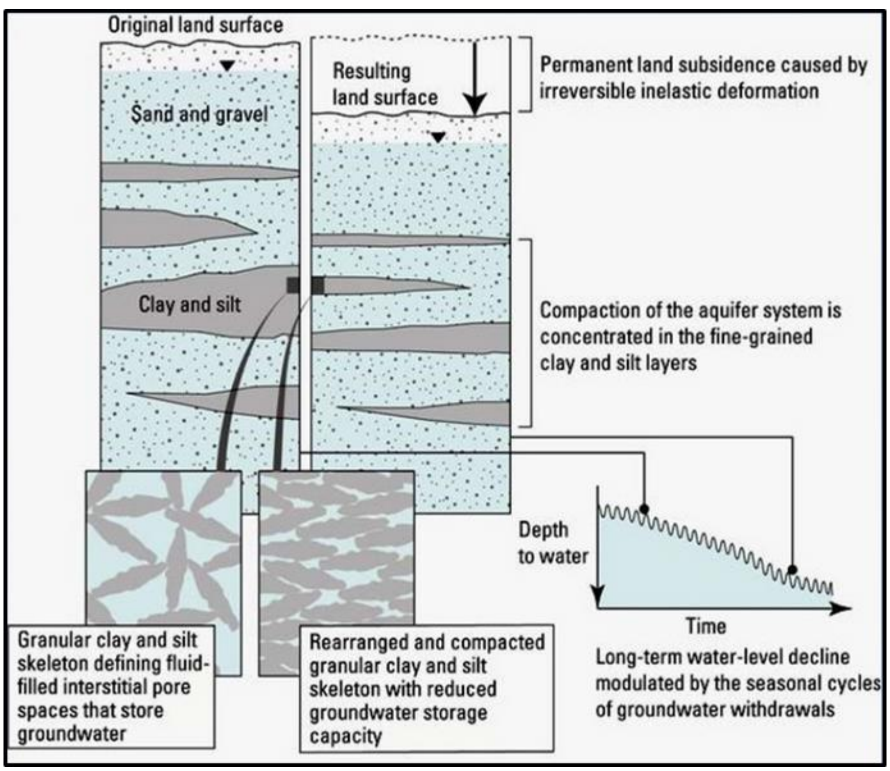

Figure 2.1 Compaction of Confining Layer (clay) (Source: Galloway et al., 1998)

Aquifers usually consist of less compressible materials i.e. sands, gravel, which do not yield as readily to stress changes and deform primarily elastically (Amelung et al., 1999, Chatterjee et al., 2006, Hanson, 1988). Water is temporarily or permanently removed from storage in the system. Particularly in confined aquifer systems a large part of the storage can be lost due to the compressibility of the aquifer system materials (Hoffman, 2003).

Compaction describes the decrease in thickness of sediments as a result of an increase in the vertical compressive stress. Compaction can be described as elastic or inelastic. If the effective stress is less than any previous maximum effective stress, compaction is elastic and can be recovered. However, if effective stress exceeds the pre-consolidation stress, compaction is inelastic and cannot be recovered (Hanson, 1988).

In this study of aquifer system compaction any horizontal deformation has not been considered. The pressure change within these layers is therefore almost exactly vertical, suggesting the one-dimensional simplification. Also, the compacting layers cannot move freely in the horizontal direction. As compacting layers are in contact with over- and underlying sediments, these may restrict the compacting units from undergoing significant horizontal deformation. Aquifer Compressibility can be defined as:

$$\alpha = -\left(\frac{\mathrm{db}}{\mathrm{b}}\right)/\mathrm{d}\sigma\mathrm{e} \tag{2.8}$$

Where α is the aquifer compressibility, db is the change in the aquifer thickness and $d\sigma_e$ is the change in effective stress. The aquifer thickness decreases with the increasing effective stress.

2.1.1 Specific storage

The specific storage S_s of a saturate aquifer is defined as the volume of water released from storage per unit volume of the aquifer per unit decline in hydraulic head. Water released from the storage due to a decrease in h is produced either by the expansion of the water caused by decreasing p or the compaction of the aquifer caused by the increasing σ_e. Specific storage S_s is the given as:

$$Ss = \rho g\ (\alpha + n\beta) \tag{2.9}$$

Where β is bulk modulus of compression, the Storativity of a confined aquifer of thickness b is the volume of water released from the storage per unit surface area of the aquifer per unit decline in hydraulic head.

$$S = Ssb \tag{2.10}$$

Which can also be written as

$$S = \rho g b \, (\alpha + n\beta) \tag{2.11}$$

Storativity values for confined aquifers varies from 0.00005 to 0.005; storativity values for unconfined aquifers are much higher, ranging from 0.02 to 0.30 (Murthy, 2002). Therefore, for the same decline in hydraulic head, the total volume of water released from an unconfined aquifer will be much greater than the volume of water released from a confined aquifer.

Compaction and expansion in multiple layered units typically contribute to the observed surface displacements over unconsolidated alluvial aquifer systems. Depending on the stresses in the aquifer system with respect to the pre-consolidation stress the observed surface displacements have to be interpreted in terms of elastic deformation or non-recoverable inelastic compaction. Large-magnitude land subsidence observed over many aquifer systems is generally due to inelastic compaction of thick, highly compressible interbeds and confining units which mainly consists of compressible silt and clay deposits.

2.1.5 Impacts of Land Subsidence

Inelastic compaction of Aquifer system is irreversible in nature leading to Land Subsidence. Many problems that land subsidence can lead to mainly includes changes in elevation, damage to structures such as buildings, railroads, roads, levees, canals and bridges; structural damage to public and private buildings; and damage to wells. In some places, Land Subsidence mostly leads to flooding (Hung et al., 2010)

2.3 Predictive Modelling

It is important to understand and predict the aquifer system’s response to stresses occurring because of the groundwater extraction to help improve the management of groundwater resources. It is very important to predict the future development of land subsidence based on present state. Several approaches to predict the land subsidence due to groundwater withdrawal according to different geological conditions and groundwater withdrawal practice have been used.

Helm in 2003 classified approaches for predicting Land Subsidence into three categories i.e. (1) Empirical methods; (2) semi-theoretical approach; (3) theoretical approach. Empirical Methods extrapolates available data to derive the future trend. SEMI-THEORETICAL method utilizes the relation between subsidence and related phenomena. Although it not completely theoretical, it can still it can be used for predicting future trend. Theoretical approach, as used in this study, is based on the relationship between compressibility of different beds and Pressure head decline.

Soil is very complex and it is difficult to handle any kind of a theoretical model of subsidence. Many simplifications and idealizations have been done in order to obtain some kind of a model that allows a more or less correct interpretation of past events, prediction of future ones, and decisions to be made about them.

Wolkersdorfer and others in 2006, also used a similar theoretical approach for predicting subsidence. Different parameters like decline in piezometric head, bulk modulus of compression of aquifer grain structure and confining layer materials and Porosity of the aquifer are important for predictive modelling using consolidation theory.

2.3.1 Elastic Compaction

Elastic and Inelastic Compaction are estimated separately based on hydraulic head change in pre and post monsoon. The following equation gives an estimate of the elastic compaction of the aquifer grain structure due to head decline (Domenico, 1972):

$$\Delta m_{aq} \; = \; \Delta P \; (\frac{S}{\gamma_w} - \beta \, * \, n \, * \, m_{aq}) \tag{2.12}$$

Where, Δm_{aq} is the change in thickness of an aquifer, m_{aq} is the original thickness, S is the storativity of the aquifer, γ_w is the specific weight of water, β is the reciprocal of bulk modulus of compression of the fluid (E_w), n is the porosity of the aquifer and ΔP is the change in the piezometric pressure due to the change in piezometric head, may be described as:

$$\Delta P = \Delta h * \rho * g \tag{2.13}$$

Storativity of the aquifer that is given as:

$$S \; = \; m_{aq} * \; \gamma_w * \alpha \tag{2.14}$$

Where, α is the reciprocal of the bulk modulus of compressibility of the aquifer grain structure (Es).

On substituting values of ΔP, S, β in equation 2.12 we get:

$$\Delta maq \; = \; \Delta h \; * \; m_{aq} \; [\left(\frac{\gamma}{E_s}\right) - \left(\frac{\gamma}{E_w}\right) \; * \; n] \tag{2.15}$$

Elastic deformation of the aquifer is not that significant in comparison with that of inelastic compaction. It is because of the decline in piezometric head, the recharge in aquifer takes place due to the expansion of the water molecules remained in the aquifer and the compression of the aquifer matrix below the aquifer (Sahu and Sikdar, 2011).

2.3.2 Inelastic Compaction

Inelastic compaction of confining layers due to piezometric head declines can be given as:

$$\Delta m_c = \frac{\gamma w}{Ec} * \Delta h * mc \tag{2.16}$$

Where, Δb_c is the change in thickness of the confining layers i.e. inelastic compaction, γ_w/E_c is the ratio of specific weight of water to bulk modulus of compression of confining layers and mc is original thickness of the confining layers.

❖ Capillary Rise

Thickness of the confining layers is a very important factor in determining the total compaction. Capillary Rise decides the height up to which the water would rise in the confining layers.

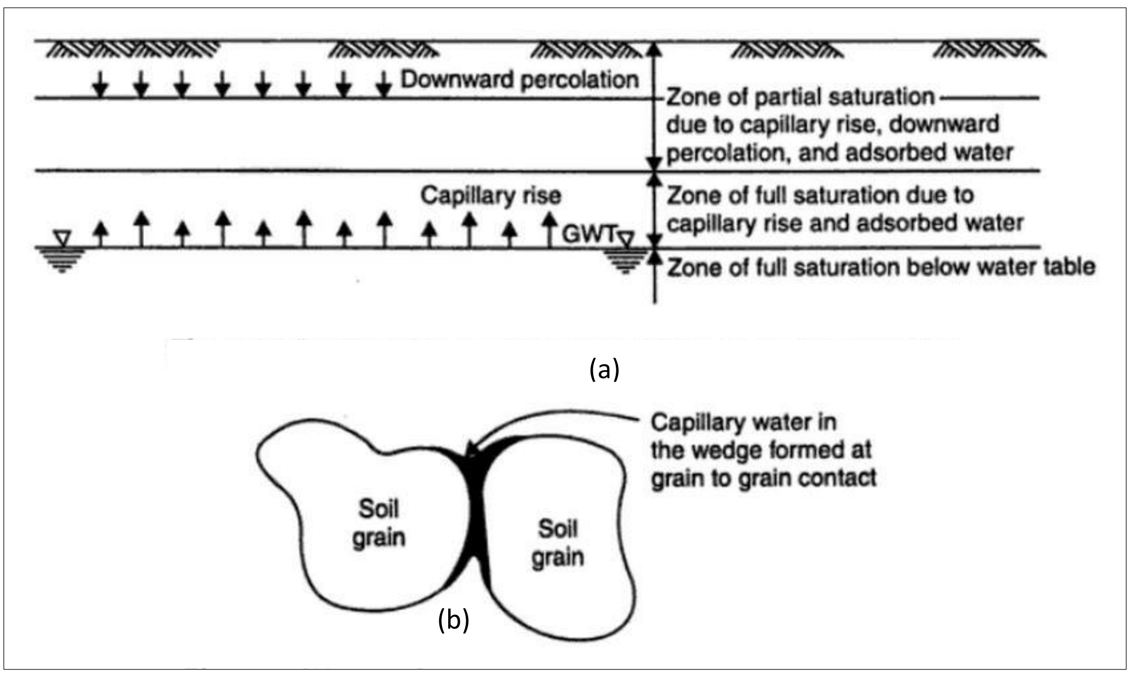

Figure 2.2 (a) Capillary fringe with zones of full and partial saturation (b) Wedge of Capillary water at the contact of soil grains (Source: Venkatramaiah)

The basic equation for capillary rise is given as:

$$h_c = \frac{2T \cos \propto}{r\gamma_w} \tag{2.17}$$

Where, h_c is capillary rise in cm T is the surface tension of water that can be taken as equal to 75 x 10~8 kN per cm, assuming a, which is contact angle between the soil and the water to be equal

to 0, r is the radius of the pore spaces expressed in centimeters and γ_w is the specific weight of water which h is equal to 9.81 kN/m3.

Since r= d/2 equation 2.17 can be rewritten as:

$$h_c = \frac{4T \cos \propto}{d\gamma_w} \tag{2.18}$$

Where, d is the pore diameter.

On substituting the values of T,∝, d, γ_w equation 2.18 can be reduced to,

$$h_c = \frac{0.3}{d} \tag{2.18}$$

The void spaces in a soil are not regular in size and shape, as they interconnect in all directions. The continuous pores in soils have a varying width. The equation 2.17 indicates the inverse relationship between the void spaces and the capillary rise (Venkatramaiah, 2006). Smaller the voids, larger would be the rise in soil grains. When water rises into the intricate network from aquifer, the lower part becomes completely saturated with water. In the upper region, water occupies the smallest voids the wider area remains filled with air. In presence of some large voids, capillary rise can effectively stop in some parts. Only smaller voids would allow water to rise up to the height h_c.

The soil above the water table might become fully saturated with water depending upon several factors. Partial Saturation Zone lies above this zone. Both these zones together constitute the capillary fringe zone. Since, the pore spaces and the grain size are of the same magnitude order, it follows that height of capillary rise would be greater in fine grained soils. The table below gives the typical range of capillary rise in different soils as given by Mc Carthy, 1977.

Table 2.1. Typical range of capillary rise in different soils as given by Mc Carthy, 1977.

Soil	Approximate Capillary Rise(mm)
Fine Gravel	20-100
Coarse Sand	150
Fine Sand	300-1000
Silt	1000-10000
Clay	10000-30000

2.4 Interferometry

2.4.1 Synthetic Aperture Radar

Synthetic Aperture Radar is a Microwave Remote Sensing technique in which microwave beams, from the antenna, are transmitted towards the surface of the earth. Using the Radar principle the backscattered energy is measured to form an image. The surface material and the size of the target can be characterized by the amplitude of the reflected wave. The two way travel time i.e. between the target and the satellite helps in measuring the distance between the two. The greater the size of the antenna, narrower is the beam and better is the resolution in the direction of flight track (Jensen, 2009). However, large antenna size is not possible. Therfore, Synthetic Aperture Radar technique is used based on the Doppler's principle. SAR makes up a virtual antenna with a big aperture size by transmitting and receiving radio waves during flight. To improve the range resolution, pulse width of a transmitting wave should be made as narrow as possible. However, a narrow pulse width has higher chance of getting interfere with noise.

SAR Image is converted from raw data to Single Look Complex (SLC) format. SLC contains both phase and amplitude information in the form of complex numbers. Amplitude represents the variation in brightness which indicate spatial variations of the physical characteristics of the ground surface whereas, phase values represents the delay in time of the received signal in a coherent system (Haldar et al., 2014). SLC is stored in slant range which can be geocoded to ground range.

SAR satellite observes in oblique direction downwards and not directly below. It is in ascending orbit (northward) that the satellite observes from west and it is in descending orbit (southward) that the satellite observes from east side. When the ground moves towards west, if satellite observes in ascending orbit (northward), the ground moves near to the satellite. In contrast, if satellite observes in descending orbit (southward), the ground moves far from the satellite.

2.4.2 SAR Interferometry

Sytheric Aperture Radar Interferomerty (InSAR) is the measurement of different parameters like topography, surface displacement and surface change from the interference of two or more SAR acquisitions over the same area. It is based on the principle of phase difference between two coherent measurements and derives the distance information from this (Woodhouse, 2005). It requires two complex SAR images of the same area, but obtained from slightly different positions with the same sensor or two similar sensors. In 1974 Graham reported was the first to use SAR image pair to form interferogram and used the phase difference thus obtained for topographic mapping.

Each pixel of the complex SAR image contains phase which is a combination of three different contributions i.e. The two-ways travel path between the sensor and the target divided the wavelength of the sensor; interaction between the incident electromagnetic waves and the scatterers within the ground resolution cell and the phase shift induced by the processing system used to focus the image.

Complex SAR images have to be coherent that can be either acquired from two antennas on the same platform separated in a direction perpendicular to the flight direction or from the same SAR antenna at different times (Zhou, X et al., 2009). The first technique is called the single pass SAR interferometry while the other is called the repeat pass interferometry. Repeat pass interferometry requires the two phase images to be co-registered to an accuracy up to 0.1 pixel so that one phase image correspond exactly to the same pixel on the other image (Zhou, X et al., 2009).

An InSAR interferogram is an image formed by the difference of two co-registered SAR phase images of the same area indicating several factors for path difference between satellite and the ground target (Meyers, 2010). Similar to a contour, a fringe is a line of equal phase in the interferogram. The total number of fringes in an interferogram is counted from a reference point where the surface deformation (displacement) is supposedly zero (Zhou, X et al., 2009).

Interferogram is a product of two complex SAR images. An InSAR interferogram(γ) is an image formed by the difference of two co-registered SAR phase images of the same area that can be defined as the normalized complex correlation coefficient of the complex electromagnetic fields s1 and s2 backscattered by the illuminated elements at positions $\rho_1 and \rho_2$ (Strozzi, T., et al., 2001) i.e.,

$$\gamma = \frac{\langle s_1 s_2^* \rangle}{\langle s_1 s_1^* \rangle \langle s_2 s_2^* \rangle} \tag{2.19}$$

Where, <s> is the average of s and s^* is the complex conjugate of s.

The coherence $|\gamma|$, a measure of the phase noise. Coherence is the relationship between waves in a beam of electromagnetic (EM) radiation. Two waves of EM radiation are coherent if they are in phase. InSAR coherence is also used to describe systems that preserve the phase of the received signal. Coherence is affected by local slope i.e., steep slopes lead to low coherence, properties of the surface being imaged i.e., vegetated or moving surfaces have low coherence, time lag between the passes in an interferogram i.e., long lags lead to low coherence, and the baseline i.e., large baselines lead to low coherence (Ichoku and Karnieli, 1998). Coherence can serve as a measure of the quality of an Interferogram. High coherence makes for attractive, not-noisy Interferogram. Coherence values ranges from 0 to 1 where 1 indicates higher coherence.

The interferometric phase is a measure of the path difference i.e.

$$\varphi = \varphi_1 - \varphi_2 = \frac{4\pi}{\lambda}[\rho_1 - \rho_2] \tag{2.20}$$

Where φ is the interferometric phase; $\varphi_1 and\ \varphi_2$ are phase of the first and the second SAR images, respectively; ρ_1 is the distance from the SAR to the scatterer by the first acquisition; ρ_2 is distance from the second acquisition; and λ is the wavelength

Coherence can be either measured over time or space since waves can de-correlate as a consequence of separation either in space or time. It is one major problem that can lead to ambiguous interferogram. It is important to maintain a certain amount of coherence so that that the phase measurement does not get affected and also to increase the effectiveness of the interferogram (Woodhouse, 2005). There are two important sources of de-correlation i.e., baseline de-correlation and temporal de-correlation. Spatial de-correlation occurs if the interferometric baseline is not exactly zero. Critical baseline is where spatial correlation factor becomes 0.

De-correlation over time is referred to as temporal de-correlation. Temporal de-correlation is only a problem for repeat pass interferometry where there is time delay between image acquisitions (Woodhouse, 2005). Temporal de-correlation occurs due to the change in the imaged surface over a period of time. These changes are prominent in vegetated areas whereas urban areas area least affected. Temporal de-correlation is also highly wavelength-dependent. Higher radar wavelengths tend to de-correlate much slower than data acquired at shorter wavelengths.

2.4.3 Differential Interferometry:

DInSAR provides information about differential changes in the range distance between the sensor and the ground target due to the displacement of the target itself. When generating an interferogram by combining two SAR images, its phase increase can be expressed as (Mora, et al., 2003)

$$\Delta\psi_{int} = \Delta\psi_{flat} + \Delta\psi_{topo} + \Delta\psi_{mov} + \Delta\psi_{atmos} + \Delta\psi_{noise} \quad (2.21)$$

Where $\Delta\psi_{flat}$ is the flat earth component related with range distance, $\Delta\psi_{topo}$is the topographic phase, $\Delta\psi_{mov}$ is the component due to the displacement of the terrain in the slant-range direction or LOS between both SAR acquisitions, $\Delta\psi_{atmos}$ is the phase related with the atmospheric artifacts, and $\Delta\psi_{noise}$ comprise degradation factors such as spatial and temporal de-correlation.

Each term in the above equation can be given as follows:

$$\Delta\psi = \frac{4\pi * B_{\perp} * r}{\lambda * \rho * tg\theta} + \frac{4\pi * B_{\perp} * h}{\lambda * \rho * sin\theta} + \frac{4\pi\Delta\rho}{\lambda} + \psi_{atmos} + \psi_{noise} + n * 2\pi \quad (2.22)$$

The n*2π represents phase ambiguity where n is a whole number, such as 1, 2, 3,… including 0;λ,θ,ρ,$B_{\perp}$,r, h and $\Delta\rho$ are radar wavelength, look angle, slant range distance of the master image, normal spatial baseline component of the data pair, slant range variation of the data pair due to orbital separation, topographic height of the given point and ground displacement parallel to the radar line-of-sight, respectively.

The basic DInSAR technique deals with the subtracting the phase of the topographic displacements which can be achieved by using external Digital Elevation Model (DEM). A synthesized interferogram is then generated from the DEM (Zohu et al., 2009). In addition, the differential interferograms can be affected by atmospheric artifacts to an enormous extent (Mora et al., 2003).

2.4.4 Differential Interferometric Processing

After importing raw data into Single Look Complex format following steps are followed:

(i)Baseline Estimation

a. Two SAR images with normal baseline very small should be selected. And, it should not exceed the critical baseline limit. ALOS-1 has a critical baseline limit of 13,000 meters whereas for Radarsat-2 is 600-1200 meters
b. Pairs with high coherence should be selected. Coherence is directly related to normal baseline. Smaller the baseline, higher is the coherence.
c. Temporal Baseline should be selected such that coherence is maintained.

(ii)Co-registration

Pixel-to-pixel coregistration is a must between common features in SAR image pairs. Thus coregistration, the alignments of SAR images from two antennas, is an essential step for the accurate determination of phase difference and for noise reduction (Li, Z., et al., 2008). Accurate coregistration ensures high quality of interferogram as it increases the coherence leading to more accurate phase in the final result (Schreiber, R., et al, 2000). The entire purpose of the coregistration is to align the samples for phase differencing

(iii) Interferogram Generation

a. Interferogram Flattening: Phase difference that may due to flat terrain should be removed from the resultant topographic phase. So, for this purpose, an interferogram is simulated for the given interferometric geometry for an ideally flat terrain. The phase of this simulated interferogram is subtracted from the interferometric phase of the given data pair.
b. Topographic Phase Removal: Topographic variations results in topographic fringes which are again removed using External DEM.

Differential Interferogram is generated which consists of the displacement phase.

(iv) Filtering

Differential Interferogram is affected by noise due to decorrelation by temporal or spatial baseline or due to atmospheric artifacts. For repeat-pass interferometry, the noise is more pronounced due to long baseline and temporal decorrelations. InSAR noise is multiplicative in nature however in the phase image has additive features. Filtering, to a large extent, reduces noise in the interferogram however, it does not enhance or recover the signal (Baran, 2003). Goldstein Filtering is an extension of the Goldstein method, significantly improves fringe visibility and reduces the noise introduced by temporal or baseline related decorrelation. Alpha is an important component in Goldstein Filtering for tuning the filter strength. Alpha, arbitrary value between 0-1 and has the biggest impact on the filter performance. Higher the value of Alpha stronger is the filtering.

(v) Phase Unwrapping

The extracted phase appears to discontinue when an extreme values of $-\pi$ or π is reached i.e. the phase then jumps to the other end. The phase of the radar echoes may only be measured up to 2π; however, the whole phase at each point in the image is needed to obtain elevations. Phase

Unwrapping, resolves this 2π ambiguity. Different phase unwrapping technologies like region growing, minimum cost flow and phase decomposition have been used however neither of them is perfect. Slow varying topographies are not a problem even if elevations are large. Rough topographies are not a problem if elevations are contained. Minimum Cost Flow is adopted when the unwrapping process becomes difficult due to the presence of large areas of low coherence or other growing limiting factors; in such cases the Minimum Cost Flow algorithm enables to obtain better results than using the Region Growing method.

2.4.5 Displacement Mapping

Points based techniques are expensive and inefficient for monitoring large areas of subsidence (Ding et al., 2004). Therefore, DInSAR is an important technique providing accurate displacement measurements. If, ground displacement of the whole pixel as a part of the image (without distortion of the pixel) along range direction - the line of sight (LOS) between the target and the sensor is there, the displacement is reflected as a phase difference with respect to the other part of image. Along range direction, moving by half a wavelength for the pixel and thus a wavelength of round trip distance for the radar signal creates one fringe i.e. 2π phase difference. Therefore, one fringe in a DInSAR Interferogram, a complete phase cycle or fringe represents radar line of sight ground displacement of $\lambda/2$, where λ is the wavelength of radar microwave pulse being used. In this work, ALOS L-Band radar data has been used which means each subsidence fringe represents minimum of 16.4 cm of displacement calculated as (Chatterjee et al., 2006):

$$\frac{\frac{\lambda}{2}}{\cos\theta} = \frac{\frac{23.5}{2}}{\cos 15}$$

Similarly RADARSAT-2, C-Band, shows a minimum deformation of 3.04 cm.

The number of fringes in an interferogram is counted from a reference point where the surface deformation (displacement) is supposed to be zero. To count fringes in the regions of fine fringes, the interferogram should to be regenerated at higher spatial resolution by means of reducing the look number or using two images of shorter time interval.

If an area on the ground is displaced by Δr in the LOS direction of the radar, the path difference between the two acquisitions, $2\Delta r$, phase of $\Delta\Phi$ given by:

$$\Delta\Phi = \left(\frac{4\pi}{\lambda}\right)\Delta r. \tag{2.23}$$

Coherence weighted LOS displacement rates as calculated from unwrapped differential interferograms of sub scene gives precise measurements. Coherence of the sub scenes is generally higher than the full scene. AS a result, phase unwrapping could be done to a better extent (Chatterjee et al., 2015). Coherence is a very important factor in deciding the quality of interferogram and assessing the deformation rates from differential interferogram. Therefore, coherence weighted subsidence rate is important. Coherence weighted algorithm takes into consideration the contribution of each interferometric pair as function of average InSAR coherence.

2.5 Field Based Instruments

2.5.1 Extensometer

Extensometer provides precise, accurate and direct measurements of aquifer system compactions at point locations. It provides the measurement of change between a reference point and the land surface in the vertical direction (Riley, 1969). This information about the deformation is important as it helps to judge the aquifer system properties (Galloway et al., 1998). It measures compaction of the aquifer system at different depths and provides great deal of information about subsidence process (Hung et al., 2010).

In spite of being highly simple in design, it provides highly accurate and precise measurements of vertical compaction of the aquifer system ((Lofgren, 1969). It mainly consist of rods, anchors, protective tubes and the most important component that is vibrating wire (VW) displacement sensors. The protective tube is installed with rods to prevent injection to rods. The cable or the pipe is connected to a digital recorder that is to frequently measure the relative distance between the ground surface and bottom of borehole. It measures variations in land surface elevation up to 1/100th of a foot daily.

The vibrating wire transducer measures the settlement and brings about the change in frequency as a result of change in different layers. Rods are connected with anchors and are installed in borehole. Anchors and anchor rods are referenced to stable ground and move up or down as per the movement in borehole. Thus, tension of vibrating wire inside the VW transducer changes. This signal is then transmitted to the VW digital readout unit and is displayed.

Extensometer have several applications including, measurement of settlement or heaving in foundations, monitoring the stability in tunnels, mines, fills and excavations, monitoring the stability in adjacent ground during long term structure construction, measurement of the deformation in abutments and retaining

2.5.2 Piezometer

Piezometer is a device used for measuring water level and pore water pressure (Wolkserdorfer and Thiem, 2006). There should be an effective link between piezometer and pore water. One of the types of Piezometer is the standpipe piezometer. It is installed in a borehole which consist of a filter tip jointed to a non-perforated solid riser pipe. The other type of piezometer includes as vibrating wire (VW) piezometers. In this filter tip is placed in a gravel zone and a bentonite seal is placed above and below the gravel to isolate the pore water pressure at the tip. The piezometric level in the piezometer indicates the pore water pressure at the level of the filter tip.

Selection of the piezometer type depends on what needs to be measured. An open hole piezometer measures the sum of all pressures along the open section of the borehole. A piezometer has to be open to water flow at the bottom and open to atmospheric pressure at the top. The intake (point of measurement) can be slotted casing or a porous piezometer tip. Measurement can be by hand dipping of a water level or by electronic measurement using a vibrating wire or diaphragm type device. A sealed piezometer measures the pressure at the point where the piezometer tip is in contact with the formation.

Also, the choice and type of piezometers depends on the location, and the distance between each piezometer, depends on the complexity of the geology, the structural elements and the geotechnical domains (Murthy, 2002). The depth of the targeted formation will determine the depth/length of the piezometer.

2.6 Review of the previous works

Galloway and others in 1998 demonstrated the use of Interferometry for detecting and quantifying land subsidence caused by the aquifer system compaction in Antelope Valley, California. InSAR results showed high correlation with subsidence patterns as detected by traditional methods like levelling. Also, the InSAR subsidence pattern were also consistent with the subsidence pattern as predicted by different groundwater flow model and aquifer system compaction.

In 2005, Strozzi with others explicitly used Differential SAR Interferometry for Land Subsidence monitoring. Using ERS data, in various sites in Italy, Mexico and Germany, deformation velocities of few mm/year to few m/year were obtained. Interferogram stacking techniques were used to get more precise results. The results were then validated with levelling results. He concluded that DInSAR results are accurate enough for operational monitoring of Land Subsidence.

Interferometric Data has noise mainly because of the temporal decorrelation which was explained by Ding and others in 2004. Performance of InSAR was accessed based on the temporal decorrelation of SAR images and the effect of atmosphere on InSAR measurements of ground subsidence. This study concluded that vegetated rugged areas easily get affected by temporal decorrelation.

For long, GPS has been used to measure subsidence and validate InSAR results. One of the study that demonstrated the use of GPS, levelling and InSAR collaterally was by Motagh and others in 2007. The study was carried out in Iran where significant subsidence had been recognized using levelling. GPS monitoring showed that around 20 cm/year subsidence occurred between 2005 to2006. Envisat InSAR results also showed similar results. This was also compared with the piezometric data and it suggested that the most probable reason could be groundwater overdraft.

Predictive Modelling of aquifer system compaction has also been successfully demonstrated. Sahu and Sikdar in 2011, estimated inelastic compaction of the aquifer system based on the Domenico’s equation using hydraulic head change in Kolkata. The mean subsidence was estimated as 3.28 cm however, the surface expression was not prominent because of the time gap between the settlement of the thick confining layer at the top and its surface expression.

Similar studies involving aquifer system compaction and monitoring land subsidence using interferometry have been carried out in several parts of the world by Amelung et al., 1999, Ng, et al., 2008, Chatterjee et al., 2006, Hung et al., 2012, Chatterjee et al., 2013 and several others.

3. Study Area

3.1 Delhi

3.1.1 Location

The National Capital Territory (NCT) of Delhi occupies an area of 1483 Sq.km. lies between latitudes 28°24' 15'' and 28° 53' 00''N and longitudes 76° 50'24" and 77° 20' 30" E. It is divided into 9 districts and 27 Tehsils/Sub-divisions.

3.1.2 Demography

According to Census, 2001 population of NCT Delhi was13.85 million as against 9.42 million as on March 1991. The population of Delhi has increased from 1.28 crores to 1.67 crores (Census, 2011) registering an increase of over 21 per cent during the period of 2001-2011.

3.1.3 Physiography and Drainage

Physiographically, in the north and east Delhi is surrounded by the Indo-Gangetic Plains, in the west by the extension of the Great Indian Thar desert and in the south by the Aravalli ranges. Delhi has a mature topography with vast gently undulatory plains with elevation between 213-305 meters above mean sea level, low linear ridges and isolated hillocks according to GSI Report. Yamuna River flows along N-S axis passing through eastern parts of Delhi. There are large number of plaeochannels and abandoned channels of river Yamuna Delhi. Topographically, Delhi is relatively flat except for the Delhi Ridge in the central portion of the region trending in NNE–SSW direction.

3.1.4 Geology and Geomorphology

Delhi rock formations mainly consist of quartzite of Alwar series of Delhi Super Group. These formations are interbedded with thin micaceous schist bands. Proterozoic rocks occur along the ridge extending from Harchandpur in Haryana in south to Wazirabad in North Delhi. The Proterozoic Rocks are covered by unconsolidated sediments of Quaternary to recent age. Denudational hills are highest order erosional surface followed by second order alluvial plane and the third is the younger alluvial.

Delhi region has been divided into three main geomorphic units: (a) Rocky Surface: It mainly includes the linear ridges and isolated hillocks which are mainly in the south-south central parts of Delhi. (b) Older Alluvial Plain: It is present on the either side of the rocky surface and further divided into different subunits: (i) Najafgarh Older Alluvial Plain (ii) Delhi Older Alluvial Plain (iii) Maidan Garhi Plain. (c) Flood Plain of Yamuna: The low lying flat surface e characterized by abandoned channels, cut-off meanders, meander scrolls, oxbow lakes, crevasse splays, point bars and channel bars. Presence of number of cut- off meanders suggests oscillatory shifting of river.

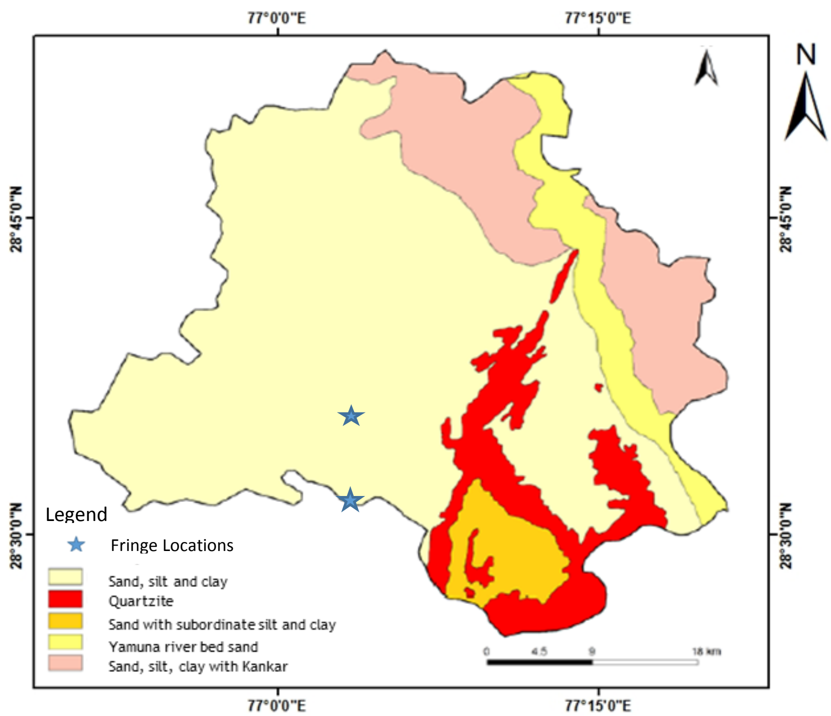

Figure 3.1. Geological Map of Delhi (Modified after GSI)

3.1.5 Groundwater Scenario

Water level, in some parts of Delhi, goes below 60 meters during pre-monsoon. South west district of Delhi has more than 46% of the well with water level below 40 meters below ground level (mbgl) and 28% wells having water level below 20 to 40 mbgl. Water level in entire Yamuna Flood plain varies between 2 to 5 meters. The Depth to water level recorded in NCT Delhi during post monsoon ranges from 0.16 to 66.10 mbgl. The depth to water level of East, North- East and North-West districts are in the range of 5-10 mbgl (Groundwater Year Book 2012-2013). The decadal fluctuation in pre-monsoon shows a decline in water levels in majority of area, with a maximum fall of 7.92 to 9.25 m in South and South West districts. The decadal fluctuation during post-monsoon also shows a decline in water level in the majority of area. Overexploitation of groundwater is at its peak in Delhi. Out of the 27 assessment units (tehsils), 2 (Daryaganj and Civil Lines) are falling in the 'Safe' Category, 5 (Gandhi Nagar, Connaught Place, Seelam Pur, Narela and Punjabi Bagh) are in the 'Semi-Critical Category while rest 20 tehsils are over-exploited.

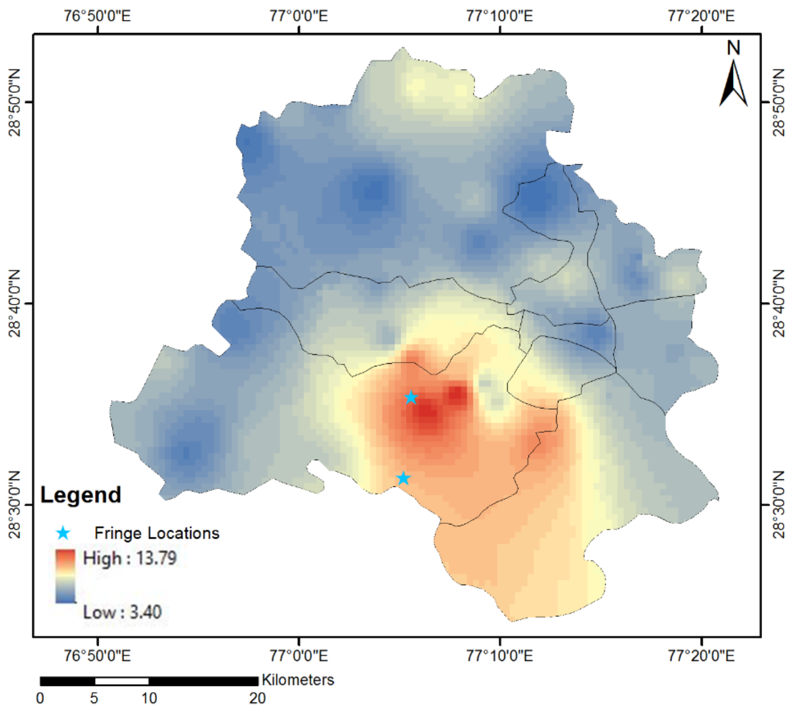

Figure 3.2. Pre-Monsoon Groundwater Depletion during 2005-2013 of Piezometric Wells, data

3.2 Chandigarh

3.2.1 Location

Chandigarh is located at the foothills of the Shiwaliks. In this study Chandigarh and its surrounding, mainly including Patiala district of Punjab, are considered for analysis lying between latitudes 30˚ 30' 00'' and 31° 00' 00''N and longitudes 76° 30'00" and 77° 20' 30" E.

3.2.2 Demography

Chandigarh has experienced great increase in population. According to Census 2011, population has increased over 10Lakhs. The main reason considered for such an increase in the rapid urbanization in the neighboring towns of Panchkula, Mohali, Khara, Zirakpur, etc.

3.2.3 Physiography & Drainage

Four major physiographic units includes, on the north eastern boundary, the NW-SE trending Siwalik hill range. The south western slopes of foothills are covered with talus material forming alluvial fans. These alluvial fans coalesce to form Kandi Formation running parallel to the hill ranges. Sukhna Choe and Patiali ki Rao, are the two streams, originating from Siwalik hill ranges forming the natural drainage of the city. Both the rivers are ephemeral and have high flows during monsoon.

3.2.4 Geology and Geomorphology

Chandigarh and its surroundings are mainly occupied by semi consolidated formations of upper Siwalik system of middle Miocene age. It majorly occupies the Indo-Gangetic Plain so mainly comprising of the alluvium of Pleistocene age. The majority is covered by the Older Alluvium consisting of layered sequence of clay, silty clay, and sand with lenses of pebbly sand and gravel. The younger Alluvium has micaceous sand and pebbles with interbeds of clay occur. The piedmont deposits at the foot of Siwalik Hills are occupied by cobble, pebble and boulder, associated with clay, silt and sand. These are followed by alluvial plain deposits.

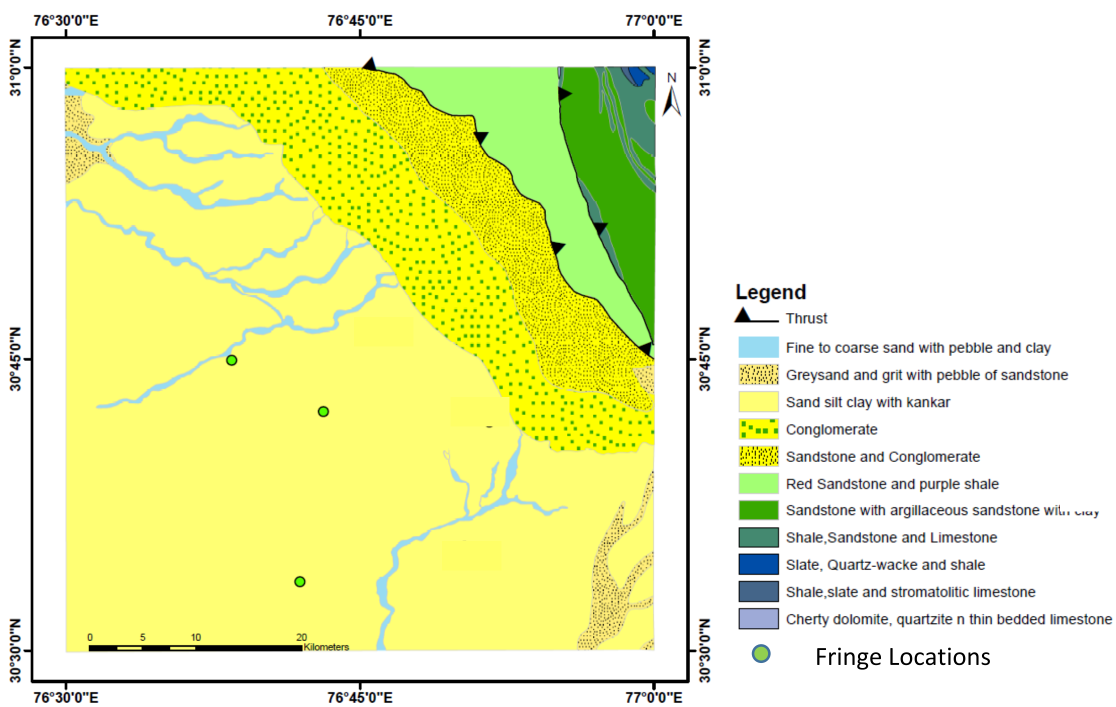

. **Figure 3.2. Geological Map of Chandigarh and surroundings (Modified after GSI)**

3.2.5 Groundwater Scenario

Levels of the deeper aquifers are in the range of 15 to 70 meters below ground level (mbgl), those in the shallow unconfined aquifer are in the range of 2 to 17 mbgl. According to CGWB, a distinct aquifer of around 10-20 m thickness at a depth of about 160 m exists persistently all over the Union Territory (UT) area except southwestern parts. The water levels are especially quite shallow in the southwestern sectors. The water level of Pre Monsoon 2013 when compared with Pre Monsoon 2012 indicates that about 73% of the wells analyzed showing a decline. The water level decline varies between 0-2 m has been observed in 67 % of the wells analyzed and 6% of wells showing fall more than 2 m. Rise in water levels is observed in 27% of the wells analyzed (Groundwater Year Book 2012-2013).

4. Data Used and Methodology

4.1 Data Used

4.1.1 Satellite Data

(a) Optical Data

1. CARTOSAT-1 *Stereo Pair*

(b) InSAR Data

1. ALOS PALSAR-Fine Beam Single Polarization (FBS) and Fine Beam Double Polarization (FBD)

The Advanced Land Observing Satellite (ALOS) was launched in 2006 by the Japan Aerospace and Exploration Agency (JAXA) and operated till May 12, 2011. ALOS carried PALSAR (Phased Array L-Band SAR) was launched into the sun-synchronous orbit and takes 100 minutes to revolve once around the earth and makes it 14 times per day. ALOS PALSAR has repeat cycle of 46 days.

Table 3.1 ALOS-1 Specifications

ALOS-1	**FBS**	**FBD**
Central Frequency	1270 MHz	1270 MHz
PRF	1500 - 2500 Hz (discrete stepping)	1500 - 2500 Hz (discrete stepping)
range Sampling Frequency	32 MHz	16 MHz
Chirp bandwidth	28 MHz	14 MHz
Polarization	HH	HV
Off-nadir angle [deg]	9.9-50.8	9.9-50.8
Incidence angle [deg]	7.9-60.0	7.9-60.0
Swath Width [Km]	40-70	40-70
Bit quantization [bits]	5	5
Data rate [Mbps]	240	240

2. RADARSAT-2

RADARSAT-2 is a follow-on to RADARSAT-1 which mission terminated in April 2013. It has the same orbit (798 km altitude sun-synchronous orbit with 6 p.m. ascending node and 6 a.m.

descending node). Some of the orbit characteristics are 24 days repeat cycle, 14.29 orbits per day, each orbit is for a duration of 100.75 minutes.

Table 3.2 RADARSAT-2 Specifications

Centre Frequency	5.405 GHz
Bandwidth	100 MHz
Polarization	HH
Polarization Isolation	> 25 dB
Aperture Length	15 m
Aperture width	1.37 m
Mass	750 kg
Deployment Mechanism	Extendable support structure (ESS)
Altitude	798 km
Inclination	98,6 degrees
Duration of one orbit	100.7 min
Descending node	6 hrs.
Ascending node	18 hrs.
Sun-synchronous	14 orbits per day

4.1.2 Digital Elevation Model

High Resolution Digital Elevation Model generated using CARTOSAT-1 Stereo Pair

4.1.3 Ancillary Data

(a) Lithologs (Source: central groundwater control board)

(b) Groundwater Level data (Source: central groundwater control board)

(c) Bulk Modulus of Compression and Porosity Values (Source: Literatures)

(d) Survey of India Toposheets No. 53D and 53H for Delhi Area. (Source: Survey of India)

(e) Geological Map of Delhi (Source: Central Ground Water Board)

(f) Geology and Geomorphological Map of Chandigarh (Source: GSI)

(g) Land Use / Land Cover Map of Delhi (Source: Bhuvan, NRSC)

4.1.4 Field Data and Ground Truth

(a) Lithologs for Dwarka

(b) Reference Extensometer Measurement

4.2 Methodology

4.2.1 DInSAR Processing

DInSAR separates the topographic phase and the displacement related phase so that the displacement can be measured which in our case is the vertical displacement i.e. subsidence. ALOS PALSAR - L Band and RADARSAT-2 C-Band data is used for DInSAR processing. In the two pass interferometric approach, the topography related term is calculated from the DEM (Strozzi et al., 2001). SAR image pairs are acquired over a period of time such that the phase change of the radar signal can be measured in the direction of radar line of sight (Hung et al., 2009).

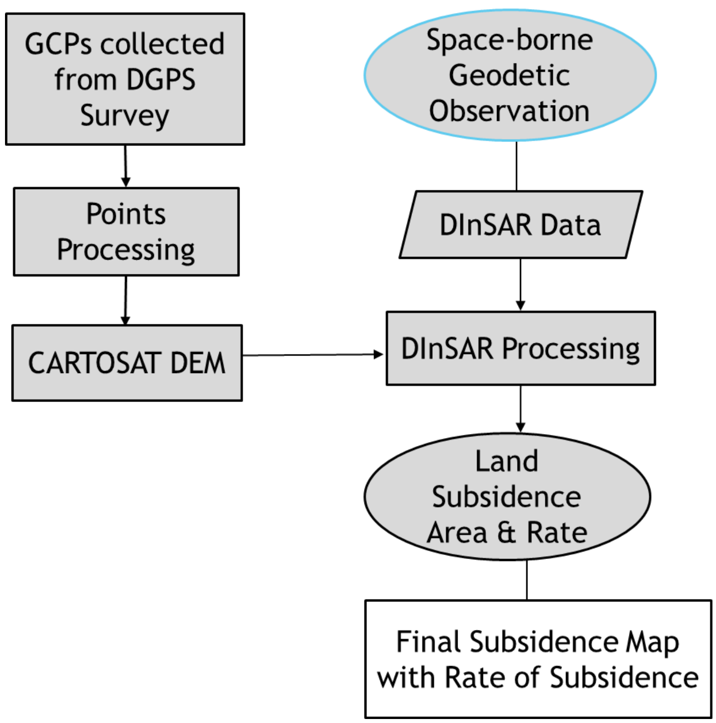

Figure 4.1. Methodology for Land Subsidence Mapping and Measurement using Interferometric Technique

The first step is to import raw data format into Single Look Complex followed by estimation of baseline. All the pairs of ALOS as well as RDARSAT-2 fall below he critical limits of spatial and temporal baseline hence used for further processing. Also, the coherence is estimated for all the pairs which is very important in deciding the quality of the interferograms. Generally, the temporal correlation decreases with increase in the time interval except in areas of high built up areas which tend to maintain a similar coherence (Ding et al., 2004). The table below highlights the details of the interferometric pairs:

Table 4.1. ALOS 1- Pairs for Interferogram Processing in Delhi

InSAR Pair	Master	Slave	Baseline Temporal (D)	Normal Baseline (meters)	Doppler Centroid diff.	Ambiguity Height(m)	Coher-ence
A1	02-12-2009	17-01-2010	46	361.596	9.116	177.194	0.44
A2	02-12-2009	04-03-2010	93	755.926	-15.61	84.761	0.32
A3	02-12-2009	20-01-2011	413.9	1831.37	-10.569	34.986	0.22
A4	17-01-2010	04-03-2010	46	530.988	-24.726	120.648	0.46
A5	17-01-2010	20-01-2011	367.9	1513.51	-19.685	42.327	0.66
A6	04-03-2010	20-01-2011	321.9	1113.55	5.04	57.536	0.23

Table 4.2. ALOS 1- Pairs for Interferogram Processing in Chandigarh

InSAR Pair	Master	Slave	Baseseline Tem-poral	Normal Baseline (meters)	Doppler Centroid diff.	Ambiguity Height(m)	Cohe-rence
B1	02-12-2009	17-01-2010	46	380.055	8.854	168.546	0.40
B2	02-12-2009	04-03-2010	92	805.01	-15.498	79.573	0.26
B3	02-12-2009	20-01-2011	413.9	1966.026	-13.227	32.582	0.15
B4	17-01-2010	04-03-2010	46	550.976	-24.352	116.299	0.62
B5	17-01-2010	20-01-2011	367.9	1629.482	-22.081	39.324	0.25
B6	04-03-2010	20-01-2011	321.9	1189.969	2.271	53.828	0.16

Table 4.3: Radarsat-2 Pairs for Interferogram Processing in Delhi

InSAR Pair	Master	Slave	Temporal Baseline (Days)	Normal Baseline	Doppler Centroid diff. (Hz)	Ambiguity height (m)
C1	3-12-2013	20-01-2014	48	55.645	-10.235	261.012
C2	3-12-2013	9-3-2014	96	282.233	58.236	51.461
C3	3-12-2013	15-01-2015	408	364.422	2.261	39.855
C4	3-12-2013	4-3-2015	456	65.098	67.807	223.11
C5	3-12-2013	21-04-2015	504	133.555	-14.24	108.749
C6	20-01-2014	9-3-2014	48	227.085	68.471	63.959
C7	20-01-2014	15-01-2015	360	419.079	12.496	34.657
C8	20-01-2014	4-3-2015	408	120.278	78.042	120.754
C9	20-01-2014	21-04-2015	456	81.883	-4.189	177.376
C10	9-3-2014	15-01-2015	312	646.173	-55.975	22.478
C11	9-3-2014	4-3-2015	360	347.202	9.572	41.833
C12	9-3-2014	21-04-2015	408	151.978	-72.66	95.57
C13	15-01-2015	4-3-2015	48	299.528	65.546	48.487
C14	15-01-2015	21-04-2015	96	497.71	-16.685	29.18
C15	4-3-2015	21-04-2015	48	198.315	-82.232	73.242

After pixel to pixel co- registration, using a DSM, topographic phase is removed and hence we get the differential interferogram. This also includes flat earth phase removal. For DSM generation, ground control points were collected over Delhi and Chandigarh using DGPS Survey. Cartosat-1 stereo pairs were used to generate 10 meter high resolution DSM. The advantage of using such is high resolution DEM is that it ensures any fringes obtained are not because of topographic effects.

Subsequently, post processing of the differential interferograms was done for highlighting differential interferometric phase. The filtering of the flattened interferogram enables to generate an output product with reduced phase noise. The sources of phase noise in the interferogram are baseline de-correlation and temporal de-correlation. Goldstein filtering was done with SNR value of 0.25. After filtering, noise was removed up to large extent.

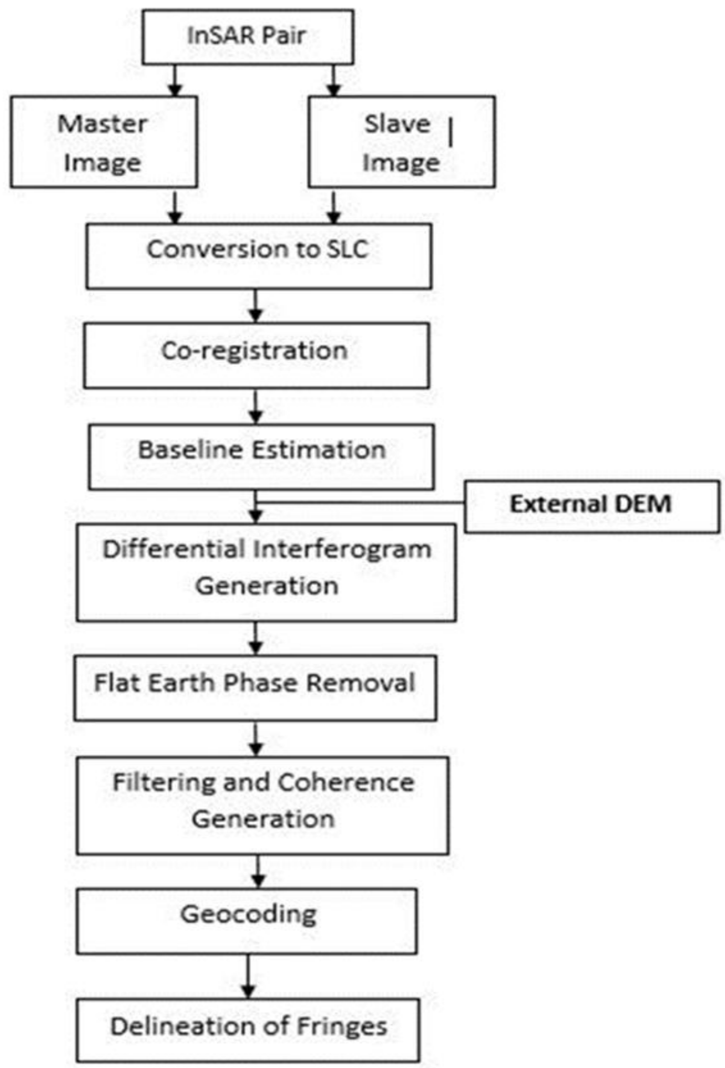

Figure 4.2. DInSAR Processing Steps

The filtered differential were subset to highlight the deformation fringes. Two sub-scenes for Delhi and 3 sub-scenes were selected for Chandigarh. Both, full scene and sub-scene processing was done which showed that sub-scene gave better results.

Filtering is followed by phase unwrapping. Phase Unwrapping is done further using Minimum Cost Flow Algorithm with Decomposition levels set as 1 and coherence threshold reduced to 0.15. The fringe analysis was performed over the geocoded filtered interferograms.

In a DInSAR Interferogram, each phase cycle i.e. 2π radians or a fringe represents λ/2 cm displacement along the radar line of sight. RADARSAT-2 C Band has wavelength of 5.6 cm therefore, LOS displacement each deformation fringe represents LOS displacement of 2.8 cm which amounts to 2.8/cos 23 or 3.04 cm of vertical deformation. Whereas, ALOS amounts to 11.8 cm LOS displacement or 11.8/cos 34.4 i.e. 14.31 cm of vertical displacement.

In this study we have used profiling technique for measuring the displacement. The component of surface displacement along the line-of-sight ($\Delta\rho$) can be calculated using the following mathematical relation as,

$$\Delta\phi = \left(\frac{4\pi}{\lambda}\right).\Delta\rho \qquad (4.1)$$

$$\text{Or, } \Delta\rho = (\Delta\phi.\ \lambda/2)/2\pi \qquad (4.\ 2)$$

To determine $\Delta\phi$, arbitrary profile was drawn in phase unwrapped image cutting across the fringe. The profile was drawn such that background could be separated from the phase. Average minimum phase was subtracted from the maximum phase to het the phase difference. To calculate rate per year: ($\Delta\rho$ * 365) Δt was done.

The rates were calculated for ALOS-1 FBS and FBD for Delhi and for RADARSAT-2 Delhi. After getting rate per year coherence based weightage has been given so that the rate estimation can be more precise.

$$RC_{12} = \frac{[(R_{12} * C_{12}) + (R_{13} * C_{13})]}{C_{12} + C_{13}} \qquad (4.3)$$

Where, RC12 is coherence weighted subsidence rate for two DInSAR fringes; R12 and R13 are the LOS displacement using absolute phase component for fringe 1 and 2 respectively; and C12 and C13 are temporal baselines for data pair 1 and 3 respectively.

4.2.2 Predictive Modelling

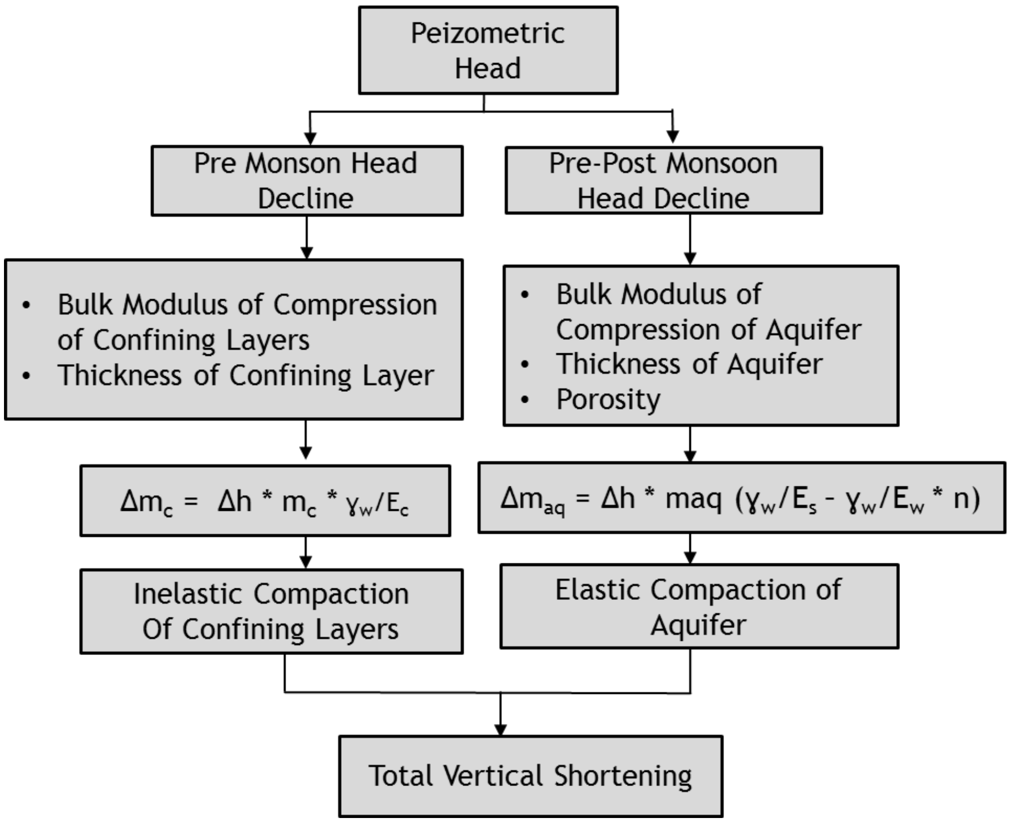

Figure 4.3. Methodology for Predictive Modelling

Areas where unconsolidated or semi-consolidated alluvial aquifers are confined or partially confined by thick fine-grained beds, are more prone to subsidence because of the decline in piezometric head due to excessive water drawdown. The relationship between pore fluid pressure change and aquifer compression as,

$$\sigma_e = \sigma_T - p \tag{4.4}$$

Where, effective or intergrannular stress (σ_e) is the difference between the total stress (σ_T) and the pore fluid pressure (p). So, according to this principle, if the effective stress is increased by decrease in pore fluid pressure and the effective stress does not exceed the maximum past effective stress, the compression is elastically however, if decrease in pore fluid pressure causes effective stress to increase to an amount greater than the previous maximum effective stress, then fine grained confining layer i.e. aquitards undergo pore volume reduction thus the compaction of the aquitards. Initially, the aquifer undergoes elastic compaction however, with continued decline in piezometric head aquitards leak water to the aquifer leading to permanent inelastic compaction.

The amount of elastic compaction in an artesian aquifer is given by Lohman's Equation (1972) as:

$$\Delta b_{aq} = \Delta P \left(\frac{S}{\gamma_w} - \beta . b_{aq} . \theta\right) \tag{4.5}$$

Where, Δb is the amount of Land Subsidence in meters, ΔP is the change in piezometric pressure in $kg/cm^{2,}$ S is the storativity of the aquifer (in decimal fraction), γ_w is the specific weight of water per unit area ($0.1\ kg\ cm^{-2}\ m^{-1}$), b is the original thickness of the confining layers, θ is the porosity and β is the bulk modulus of compression of water ($4.74 * 10^{-5}\ cm^2\ kg^{-1}$).

ΔP, decline in piezometric pressure is due to the decline in piezometric head can be calculated as follows:

$$\Delta \mathrm{P} = \Delta \mathrm{h} . \rho_{\mathrm{w}} . g \tag{4.6}$$

Where Δh is the Piezometric head decline, ρ_w is the density of water and g is the acceleration due to gravity.

S, Storativity is the product of aquifer thickness and specific storage given as:

$$S = b_{aq} . \gamma_w . \alpha \tag{4.7}$$

Where α represents the vertical compressibility of the aquifer and is estimated as the reciprocal of bulk modulus of compression of the aquifer grain structure or $1/E_s$ where E_s is the bulk modulus of compression of the aquifer grain structure. E_s is the rate of change in the aquifer volume or aquifer thickness for a corresponding change in inter-granular pressure. Confined aquifer, storativity varies with specific storage and its thickness, typically ranges from 5x10-5 to 5x10-3 (Todd, 1980); in storativity of unconfined aquifer ranges from 0.1-0.3 (Lohman, 1972).

On substituting the value of ΔP and S in equation 2, the elastic compression of the aquifer due to piezometric head decline can be estimated as follows:

$$\Delta b_{aq} = \gamma_w . \Delta h . b_{aq} (\alpha - \beta . \theta) \tag{4.8}$$

Or
$$\Delta b_{aq} = \Delta h.\, b_{aq}(\frac{\gamma_w}{E_s} - \frac{\gamma_w}{E_w}.\,\theta) \tag{4.9}$$

Where, γ_w/E_s is the ratio of specific weight of water (γ_w) to bulk modulus of compression of aquifer grain structure and γ_w/E_w is the ratio of the specific weight of water (γ_w) to bulk modulus of compression of water.

To estimate the amount of inelastic compaction leading to land subsidence, vertical shortening of a column of confining layers has to be estimated. Capillary rise plays an important role in deciding the height of the column up to which the water would rise. In general, capillary rise in a tube is given as follows:

$$h_c = \frac{4T_s\, cos\alpha}{d\gamma_w} \tag{4.10}$$

Where h_c is the capillary rise above the water level, T_s is the surface tension along the line of contact between the meniscus in a tube and the walls of the tube itself, α is the contact angle between the meniscus and the tube, d is the diameter of the tube and γ_w is the specific weight of water. However, in soils voids have different width. The portion of the soil immediately above the water table becomes saturated with water whereas the portion above remains saturated with air. The smaller the pore spaces, higher is the capillary rise however, the rate of rise is very slow because of the low permeability (Murthy, 2002). As the effective grain size tends to decrease, the void size also decreases, and the height of capillary rise can be determined from the equation,

$$h_c = \frac{0.3}{d} \tag{4.11}$$

Where, d is the pore diameter in centimeters. Permanent aquifer system compaction i.e. inelastic compaction and land subsidence result from a decline in aquifer hydraulic head below the critical head that causes an increase in the effective stress to values greater than past effective stress (Galloway et al., 1998):

$$\Delta b_c = \frac{\gamma_w}{E_c}.\, \Delta h.\, m_c \tag{4.12}$$

Where, Δb_c is the change in thickness of the confining layers i.e. inelastic compaction, $\frac{\gamma_w}{E_c}$ is the ratio of specific weight of water to bulk modulus of compression of confining layers and mc is original thickness of the confining layers.

(a) CGWB data

12 piezometric wells spread across Delhi were used for estimation. For inelastic and elastic compaction, Pre-Monsoon and post-monsoon head change (Δh) was calculated respectively. Original thickness of the aquifer (b_{aq}) and the confining layers (b_c) was calculated from Lithologs. In study we have considered only the first aquifer therefore, the maximum depth considered for both the wells is 36 meters.

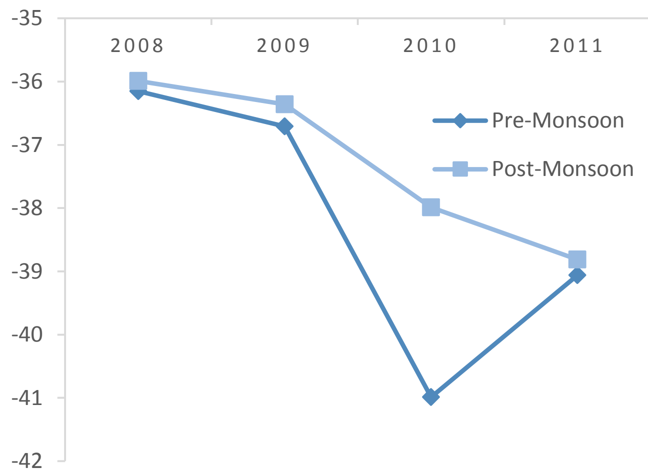

Figure4.3. Piezometric Head Change in Well 1, Dwarka

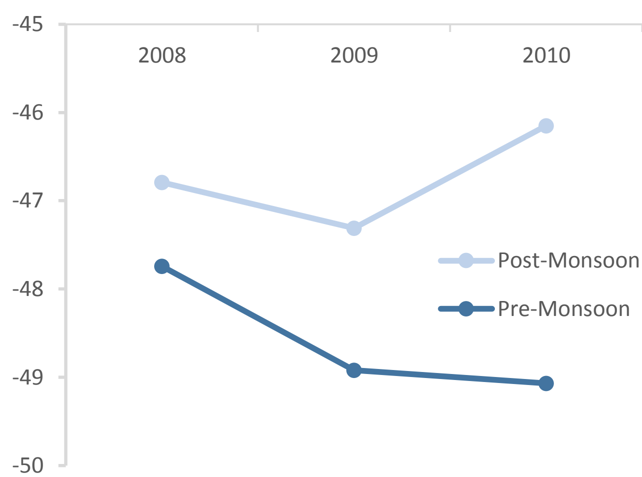

Figure4.4. Piezometric Head Change in Well 2, Gurgaon

Piezometric head decline (Δh), for elastic compaction is calculated by subtracting pre-monsoon from the post-monsoon water level. For inelastic compaction, re-monsoon water level is subtracted from the previous year's water level. Variations in the water level of the two well is given below.

The value of γ_w/E_s i.e. the ratio of specific weight of water to bulk modulus of compression of aquifer grain structure is taken from literatures which are as follows:

Table 4.4 Specific Storage values adapted from Domenico and Mufflin (1965)

Porous Material	Modulus of Elasticity E_s(N/m2)	Specific Storage(γ_w/E) S_s(m-1)
Plastic Clay	$4.78 * 10^5$- $3.82 * 10^6$	$2.03 * 10^{-3}$- $2.56 * 10^{-3}$
Stiff Clay	$3.82 * 10^6$- $7.65 * 10^6$	$2.56 * 10^{-3}$- $1.28 * 10^{-3}$
Medium hard clay	$7.65 * 10^6$- $1.43 * 10^7$	$1.28 * 10^{-3}$- $9.19 * 10^{-4}$
Loose sand	$9.56 * 10^5$- $1.91 * 10^7$	$1.02 * 10^{-3}$- $4.92 * 10^{-4}$
Dense Sand	$4.78 * 10^7$- $7.65 * 10^7$	$2.03 * 10^{-4}$- $1.28 * 10^{-4}$
Dense sandy gravel	$9.56 * 10^7$- $1.91 * 10^8$	$1.02 * 10^{-4}$- $4.92 * 10^{-5}$
Rock, fissured, jointed	$1.43 * 10^8$- $2.99 * 10^9$	$6.89 * 10^{-5}$- $3.28 * 10^{-6}$
Rock, sound	Greater than $2.99* 10^9$	Less than $3.28 * 10^{-6}$

The value of γ_w/E_w i.e. the ratio of the specific weight of water (γ_w) to bulk modulus of compression of water is $4.74 * 10^{-5}$ cm^2 kg^{-1}.

Using equation 4.9 and 4.12along with the input data, we have calculated elastic and inelastic compaction for each well and in a year and summed them up to get the total vertical shortening. Cumulative subsidence is calculated over a period of four years to get the overall scenario.

Similar process was repeated for the soil samples obtained from the site where extensometer has been drilled

Table 4.5 Capillary Rise as observed in some of the porous material

Porous Material	Grain Size(mm)	Pore Diameter(mm)	Capillary Rise (meters)
Sandy Silt	0.1	0.0086	3.488
Sandy Silt to Fine Sand	0.2	0.0344	0.872
Silt	0.063	0.0034	8.789
Sandy Silt, Silt and minor sand grains	0.5	0.2150	0.139
Sandy Silt	0.1	0.0086	3.488
silty clay	0.04	0.0013	21.80
sand	1.5	1.935	0.015

(b) Soil Samples

Based on the soil samples obtained from the field the above procedure was again repeated to get the compaction values at the particular location. The target aquifers are found at a depth of 30-33, 40-42 and 58-70 meters respectively. The confining layers mainly consist of silt and fine sand.

4.2.3 Field Measurements

Vibrating wire Extensometer installed at Dwarka (a) location. The well was drilled up to 81 meters. Important aquifers were at a depth of 40-42 and 58-70 meters. The extensometer has 5 sensors. So, depending upon the requirement the five sensors were placed at a depth of 20, 39.5, 43.5, 59.5 and 78 meters.

Also, piezometer has been installed at the same site for getting the pore pressure. The bottom is filled with the bentonite mud. Sensor is placed at a point such that we get the maximum pore pressure.

5. Results and Discussion

5.1 DInSAR Mapping and Measurements

DInSAR technique has shown high potential of mapping subsidence with cm/year level of accuracy. In this study ALOS-1 and RADARSAT-2 has been used to map and monitor Land Subsidence over Delhi and Chandigarh.

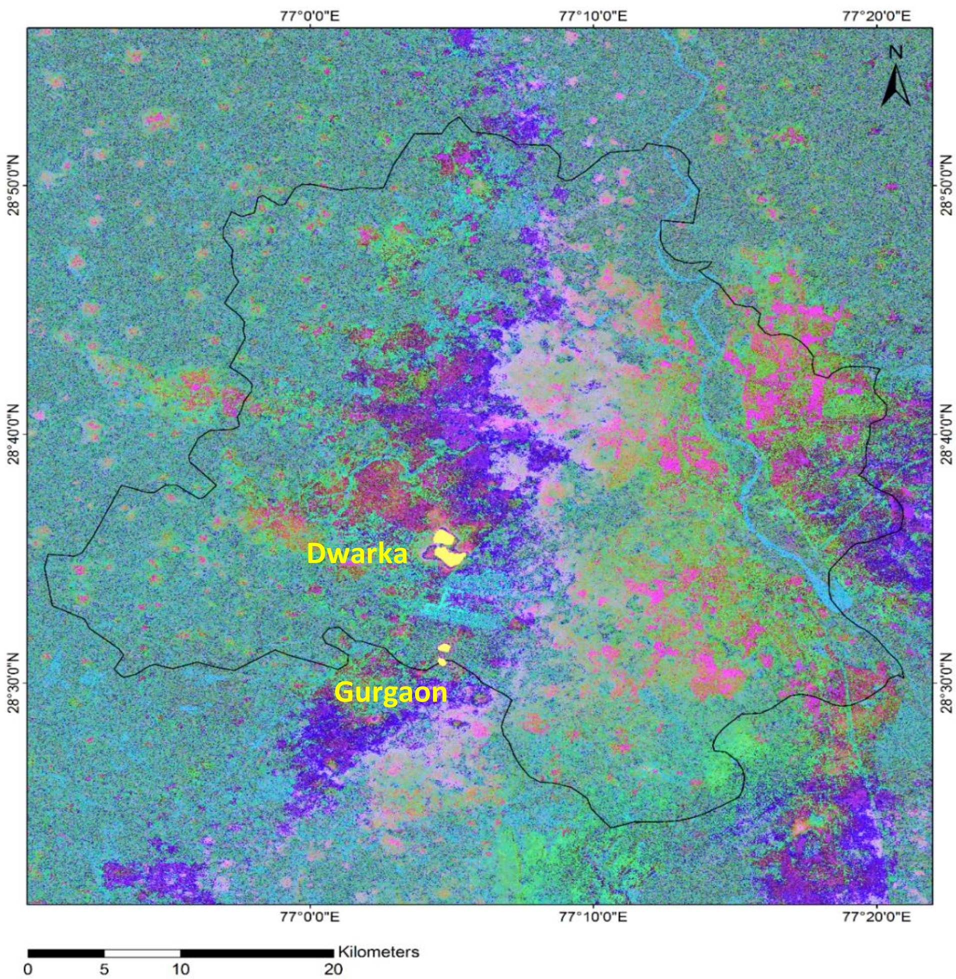

Figure 5.1. RADARSAT-2 displayed with HIS inverse transform where amplitude is assigned as intensity, interferogram as hue and coherence as saturation in Delhi

It is observed that the InSAR high coherence is maintained over the fringe areas in all the ALOS-1(Table 5.1) and RADARSAT-2 (Table 5.5) InSAR data pairs. Deformation fringes appeared prominently in filtered differential interferograms in which topographic phase and noise were removed (Figure 5.3.). DInSAR phase was fused with SAR amplitude and InSAR coherence images in HIS color space for improved visualization and geographic localization of the deformation fringes (Figure 5.1).

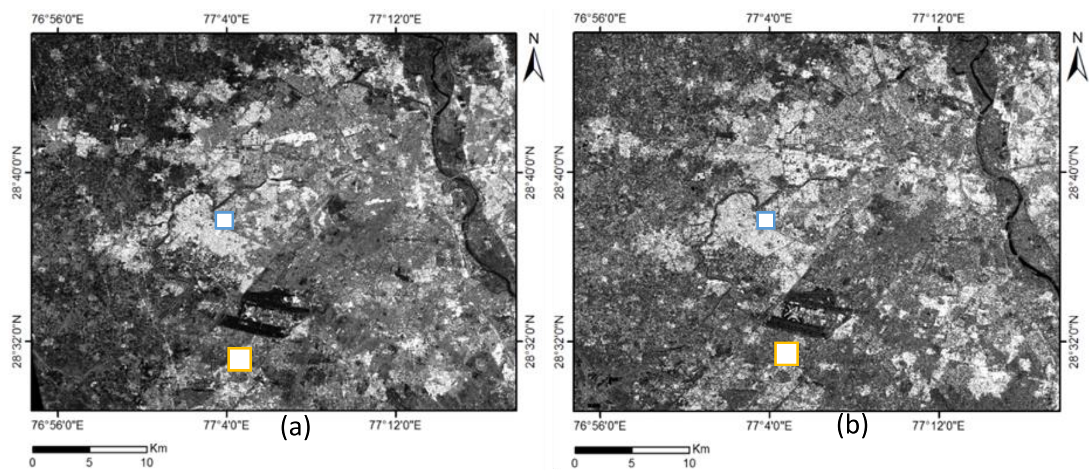

Figure 5.1. Amplitude Images (Dwarka) of the (a) master scene of the L-Band ALOS InSAR Pair A3 and (b) the C-Band RADARSAT-2 InSAR pair C3

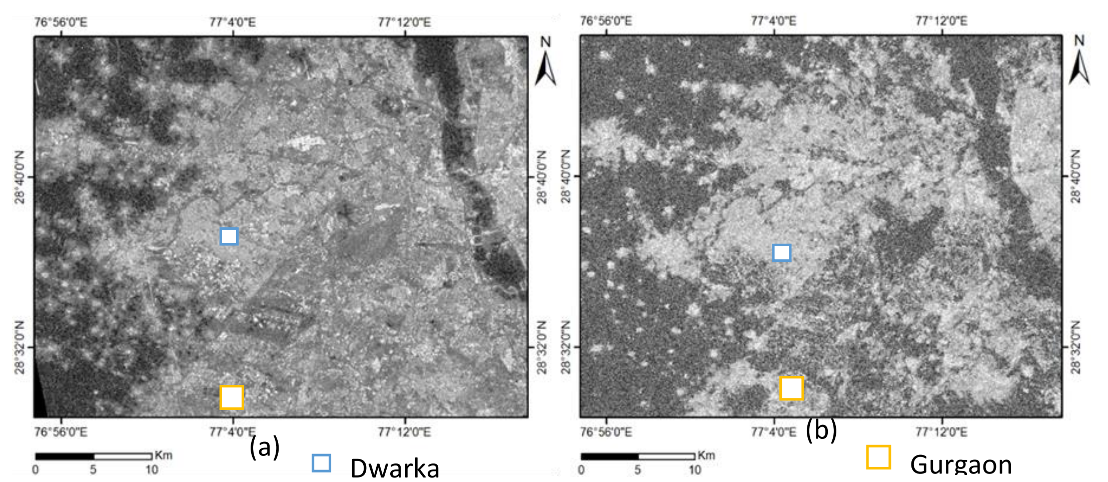

Figure 5.2. Coherence Images (Dwarka) of (a) ALOS-InSAR Pair A3 (b) RADARSAT-2 InSAR Pair C3

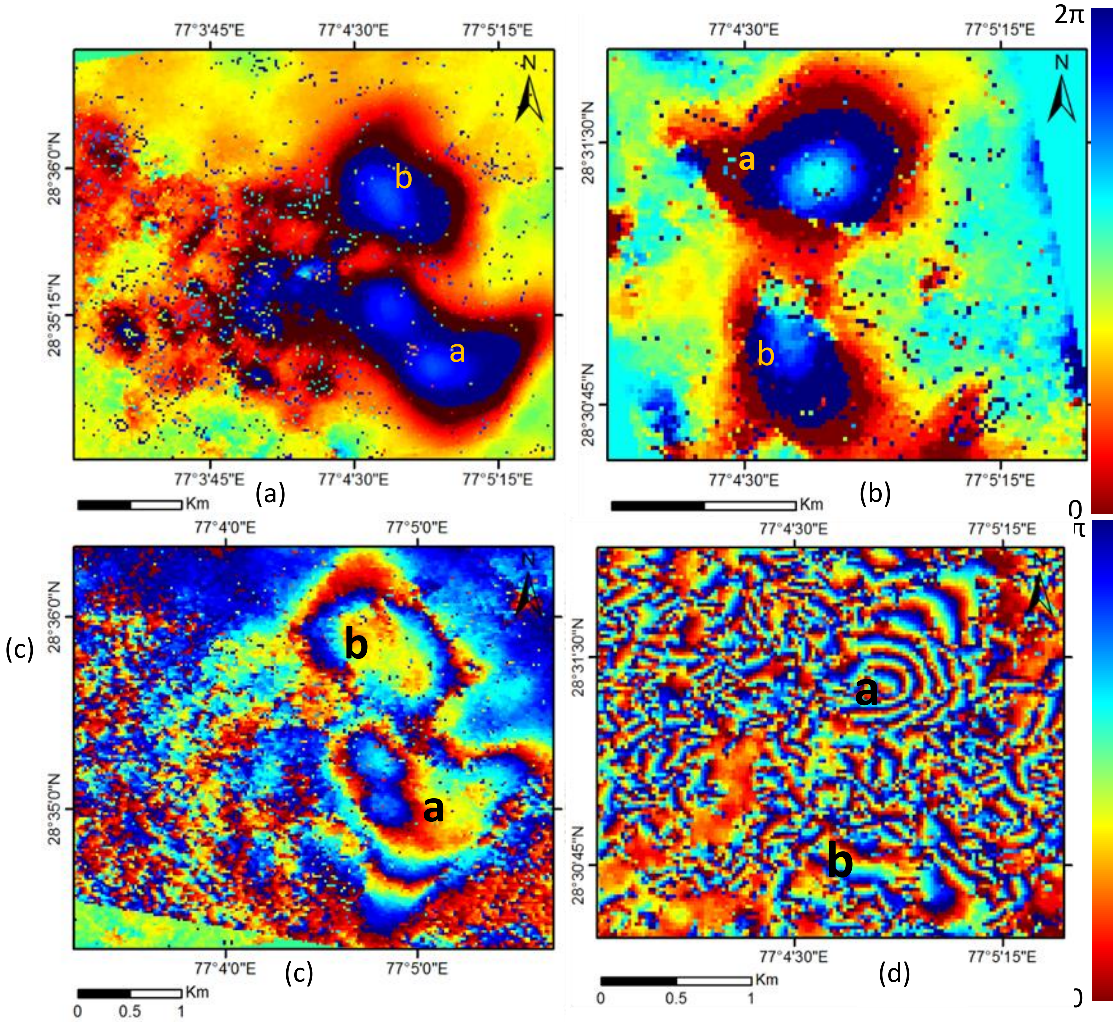

Figure 5.3. Post-Processed filtered interferogram of (a) ALOS InSAR pair A3, Dwarka (b) ALOS InSAR pair A3, Gurgaon (c) RADARSAT-2 InSAR pair C3, Dwarka (d) RADARSAT-2 InSAR pair C3, Gurgaon

L-Band differential interferogram shows well-defined deformation fringes in Dwarka, Gurgaon, Kharar, Mohali and Banur during 2009-2013 (Figure 5.3 and Figure 5.4). C-Band data also shows fringes in Dwarka and Gurgaon during 2013-2015. The phase difference in the differential interferograms represent subsidence areas.

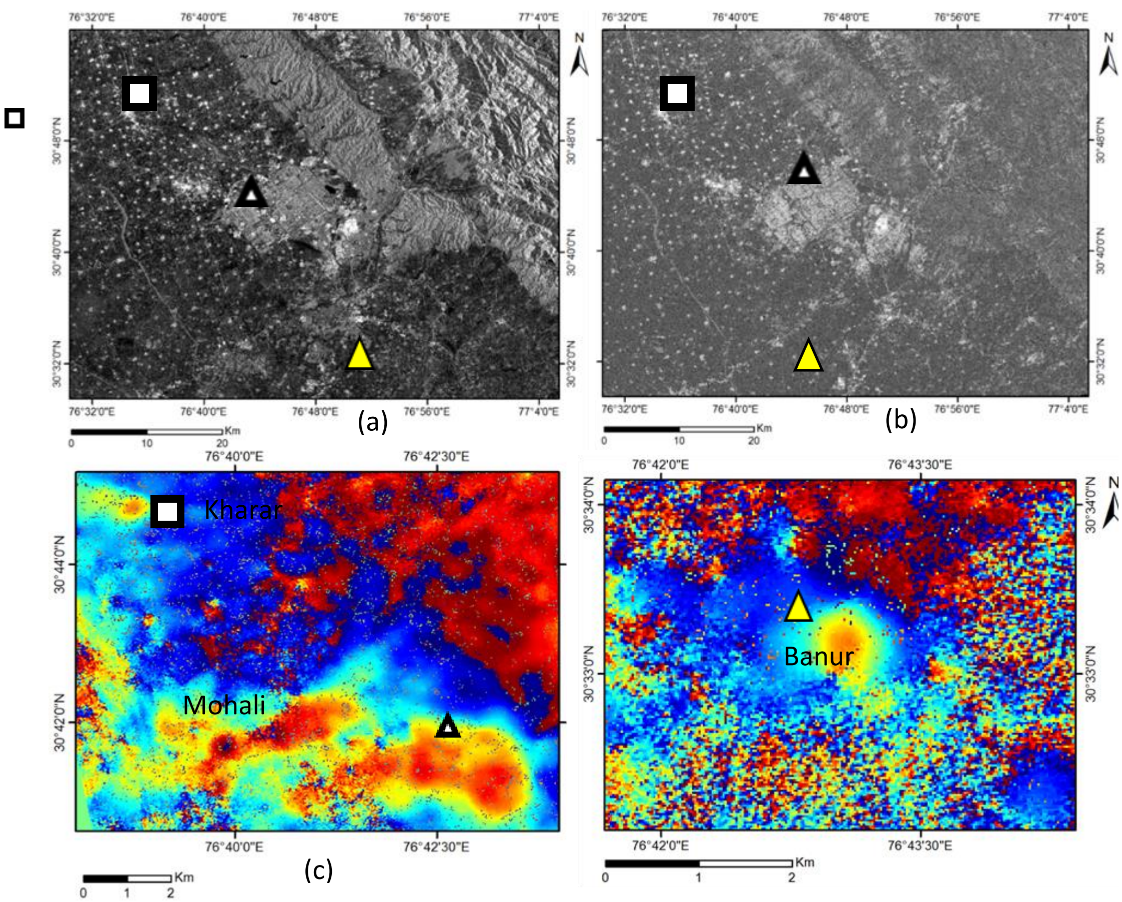

Figure 5.4. ALOS InSAR pair B3 (a) Amplitude image of master scene, (b) Coherence image, (c) subset differential interferogram of Fringe1 and (d) Fringe 2.

Deformation phase in each fringe is calculated from the unwrapped differential interferogram by phase profiling technique. ALOS-FBS, coherence weighted average deformation for Dwarka and Gurgaon is 5.7 cm/year and 5.9 cm/year respectively. For ALOS-FBD it is 5.9 cm/year for Dwarka during 200-2011. RADARSAT-2 gives average deformation rate of 5.0 cm/year for Dwarka. Displacement rates in some C-Band InSAR pairs is higher (Data pairs C8 and C12) for short temporal baseline than the pairs with longer baseline (Table 5.5).

Profiling

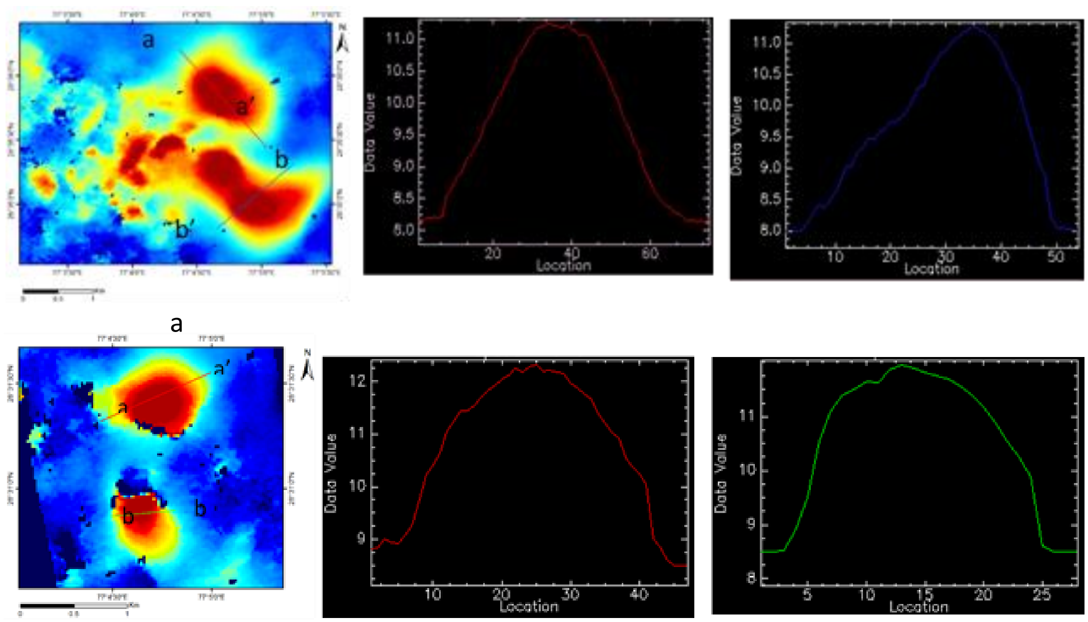

Figure 5.5. (a) ALOS phase unwrapped image for InSAR pair A3, Dwarka (b) Spatial Profiles, Dwarka (c)) ALOS phase unwrapped image for InSAR pair A3, Gurgaon and (d) Spatial Profiles, Gurgaon

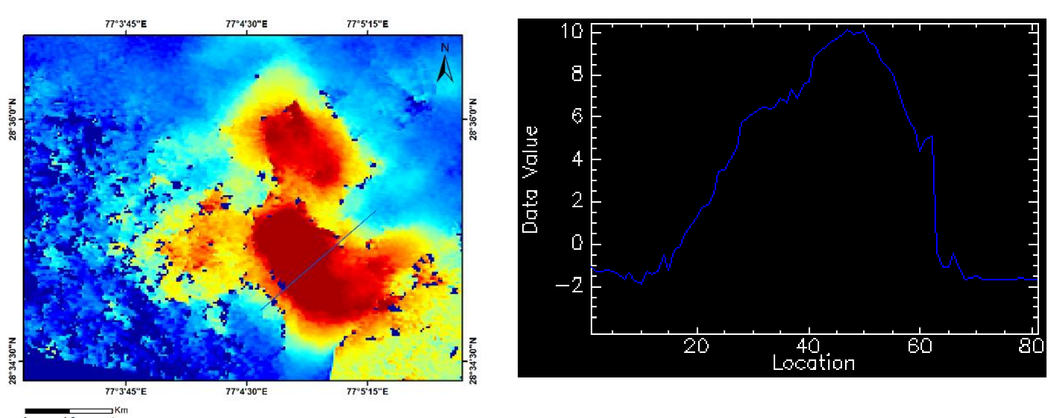

Figure 5.6 (a) RADARSAT-2 phase unwrapped image for InSAR pair A3, Dwarka (b) Spatial Profiles, Dwarka (c)) ALOS phase unwrapped image for InSAR pair A3, Gurgaon and (d) Spatial Profiles, Gurgaon

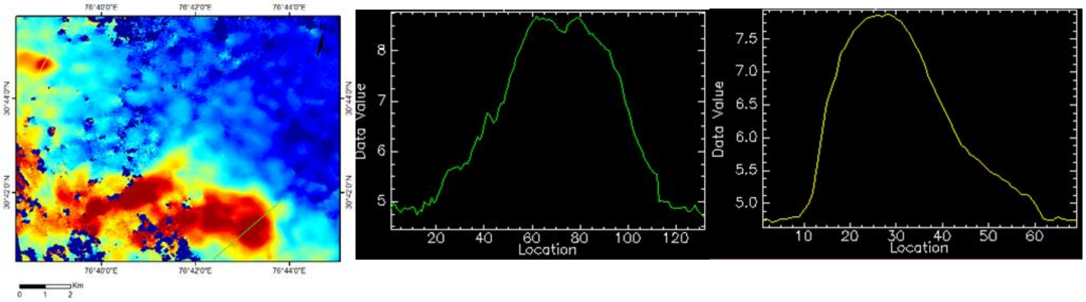

Figure 5.7. (a) ALOS phase unwrapped image for InSAR pair A3, Chandigarh(b) Spatial Profile, Mohali (c)) Spatial Profile, Kharar

<u>DInSAR Measurement Rates</u>

Table 5.1. Coherence Weighted Deformation Rates for Dwarka from ALOS-1 FBS Data

ID	Pair	Avg. Min Phase	Max Phase	Phase Difference	Path Difference	Temporal Baseline	Rate	Coh-erence
a	2009-2011	8.20	11.23	3.04	5.68	414.00	5.0	0.37
a	2009-201001	9.40	9.85	0.45	0.84	46.00	6.7	0.56
a	2009-201003	9.24	10.05	0.81	1.52	93.00	6.0	0.48
a	2010-2010	6.17	6.52	0.35	0.66	46.00	5.2	0.53
a	201001-2011	4.70	7.02	2.32	4.34	368.00	4.3	0.39
a	201003-2011	5.10	7.37	2.27	4.25	322.00	4.8	0.40
b	2009-2011	7.06	11.21	4.15	7.77	414.00	6.9	0.37
b	2009-201001	9.40	9.87	0.47	0.88	46.00	7.0	0.56
b	2009-201003	9.30	10.09	0.80	1.49	93.00	5.9	0.48
b	2010-2010	6.16	6.55	0.39	0.72	46.00	5.8	0.53
b	201001-2011	3.02	7.61	4.59	5.65	368.00	5.6	0.39
b	201003-2011	5.03	7.13	2.10	3.94	322.00	4.5	0.40

The average coherence weighted rate for fringe Dwarka (a) is 5.9 cm/year and for Dwarka (b) is 5.4 cm/year. The overall average rate for Dwarka is 5.7 cm/year.

Table 5.2. Coherence Weighted Deformation Rates for Gurgaon from ALOS-1 FBS Data

ID	Pair	Avg Min Phase	Max Phase	Phase Difference	Path Difference	Temporal Baseline	Rate	Coherence
a	2009-2011	8.66	12.27	3.61	6.75	414.00	6.0	0.34
a	2009-201001	3.20	3.68	0.48	0.90	46.00	7.1	0.52
a	2009-201003	3.20	4.06	0.87	1.62	93.00	6.4	0.43
a	2010-2010	6.30	6.65	0.35	0.65	46.00	5.2	0.46
a	201001-2011	5.00	8.09	3.09	5.78	368.00	5.7	0.35
a	201003-2011	4.60	7.35	2.75	5.14	322.00	5.8	0.36
b	2009-2011	8.50	11.94	3.44	6.43	414.00	5.7	0.34
b	2009-201001	3.19	3.61	0.42	0.79	46.00	6.2	0.52
b	2009-201003	3.30	3.94	0.64	1.20	93.00	4.7	0.43
b	2010-2010	6.27	6.59	0.32	0.60	46.00	4.8	0.46
b	201001-2011	5.05	7.52	2.47	4.62	368.00	4.6	0.35
b	201003-2011	3.97	8.00	4.03	7.54	322.00	8.5	0.36

The average coherence weighted rate for fringe Gurgaon (a) is 5.6cm/year and for Gurgaon (b) is 5.8 cm/year. The overall average rate for Gurgaon is 5.9 cm/year.

Table 5.3. Coherence Weighted Deformation Rates for Dwarka(a) from ALOS-1 FBD (HV) Data

Pair	Avg Min Phase	Max Phase	Phase Difference	Path Difference	Temporal Baseline	Rate	Cohe-rence
200909-201009	0.80	4.12	3.33	6.22	366.00	6.2	0.37
200909-201007	2.15	4.70	2.55	4.77	323.00	5.4	0.39
200910-201007	-2.06	0.97	3.03	5.66	277.00	7.5	0.39
200910-201007	-2.28	-0.06	2.22	4.15	323.00	4.7	0.35

The average coherence weighted rate for fringe Dwarka (a) is 5.9 cm/year.

Table 5.4. Coherence Weighted Deformation Rates for Kharar and Mohali from ALOS-1 FBS Data

Location	Pair	Avg Min Phase	Max Phase	Phase Difference	Path Difference	Temporal Baseline	Rate	Cohe-rence
Kharar	2009-2011	4.37	7.91	3.54	6.62	414.00	5.8	0.31
Kharar	201001-2011	5.78	8.51	2.73	5.10	368.00	5.1	0.32
Kharar	201003-2011	5.94	8.52	2.59	4.84	322.00	5.5	0.32
Mohali	2009-2012	4.91	8.66	3.75	7.01	414.00	6.2	0.31
Mohali	201001-2011	5.99	7.81	1.82	3.40	368.00	3.4	0.32
Mohali	201003-2011	5.99	8.92	2.93	5.48	322.00	6.2	0.32

Table 5.5. Coherence Weighted Deformation Rates of Dwarka (a) area of Delhi RADARSAT-2 data during 2013-2015.

Pair	Avg. Min Phase	Max Phase	Phase Diff	Path Diff	Rate	Temporal Baseline3	Coherence
2013-201503	7.85	17.41	9.56	4.41	3.5	456.00	0.52
2013-201403	1.98	4.72	2.74	1.27	4.8	96.00	0.50
2013-201401	3.40	4.86	1.46	0.67	5.1	48.00	0.64
2013-201501	9.46	11.46	2.00	0.92	0.8	408.00	0.4
2013-201504	10.15	23.24	13.10	6.05	4.4	504.00	0.53
2014-201501	13.09	13.30	0.21	0.10	0.1	360.00	0.47
201401-201503	8.02	11.54	3.53	1.63	1.5	408.00	0.52
201401-201403	-1.06	0.47	1.53	0.71	5.4	48.00	0.60
201401-201504	5.60	18.05	12.45	5.75	4.6	456.00	0.54
201403-2015	6.95	13.38	6.43	2.97	3.5	312.00	0.44
201403-201503	0.55	11.96	11.41	5.27	5.3	360.00	0.48
201403-201504	6.85	17.91	11.06	5.11	4.6	408.00	0.51
201501-201503	1.99	6.79	4.80	2.22	16.9	48.00	0.58
201501-201504	4.45	5.92	1.47	0.68	2.6	96.00	0.49
201503-201504	5.80	6.65	0.85	0.39	3.0	48.00	0.57

The average deformation rate for Dwarka (a) is 5.0 cm/year.

5.2 Predictive Modelling

(a) CGWB data

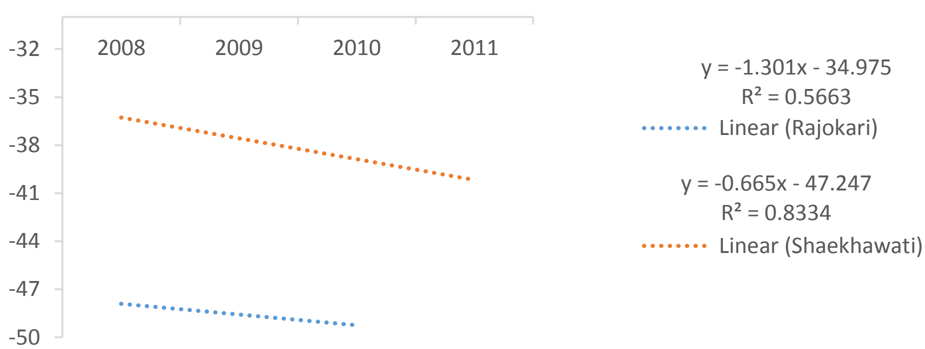

Figure 5.8. Trend line of pre-monsoon water table data

Table 5.6. Inelastic Compaction for each well in Delhi

Location	Min(cm)	Avg.(cm)	Max(cm)
Anand Vihar	0.2	0.2	0.3
BBMB Narela	0.1	0.2	0.2
Chandrawal	2.2	2.6	3.0
Dilshad Garden	3.3	3.9	4.5
Ghazipur Crossing Flood	0.3	0.3	0.4
Hauz Khash Enclave	4.9	5.8	6.8
IGI Air Port	5.6	6.6	7.7
Kingswy Camp	0.9	1.1	1.2
Nangal Dairy	9.7	11.5	13.4
NICOLSON RANGE	0.1	0.1	0.1
RAJOKRI	7.3	8.7	10.1
SECTOR-12, DWARKA	9.9	11.9	13.8

Table 5.7. Elastic Compaction at each well in Delhi

Location	Min(cm)	Avg.(cm)	Max(cm)
Anand Vihar	1.1	1.3	1.7
BBMB Narela	0.6	0.9	1.3
Chandrawal	0.6	0.8	1.3
Dilshad Garden	2.4	2.9	4.9
Ghazipur Crossing Flood	0.3	0.3	0.5
Hauz Khash Enclave	5.7	8.5	11.9
IGI Air Port	8.0	12.3	16.7
Kingswy Camp	0.2	0.2	0.3
Nangal Dairy	1.4	1.4	2.8
NICOLSON RANGE	0.4	0.5	0.9
RAJOKRI	1.2	2.4	1.6
SECTOR-12, DWARKA	1.0	4.7	1.5

Table 5.8. Potential Land Subsidence Scenario due to Aquifer System Compaction in Well 1 and 2 during 2008-2011 showing elastic compaction of the aquifer, inelastic compaction of the confining layers and total compaction of the aquifer system.

Location	Average Piezometric decline (m/year)	Thickness of the aquifer	Thickness of the confining layers Due to capillary rise (meters)	Elastic Compaction of the aquifer cm/year (Min-Max)	Inelastic Compaction cm/year (Min-Max)	Total Compaction Cm/year (Min-Max)
Dwaraka (Well 1)	1.7	15.2	18.2	0.5 (0.32-1.58)	3.9 (3.30-4.58)	4.4 (3.62-6.16)
Gurgaon (Well 2)	0.7	15	21	0.5 (0.39-0.81)	2.9 (2.42-3.37)	2.1 (2.81-4.18)

(a) Soil Samples

Elastic an inelastic Compaction calculated from the Lithologs as obtained from the drill site.

Table 5.9. Inelastic and Elastic Compaction for Soil Samples of Dwarka area

Year	Elastic	Inelastic
2008	1.2 (0.7-1.5)	1.4 (0.6-2.1)
2009	0. 8 (0.7-1.5)	1.4 (0.65-2.1)
2010	1.3 (0.8-1.7)	1.6 (0.73-2.39)
2011	2.0 (1.2-2.6)	2.4 (1.1-3.6)

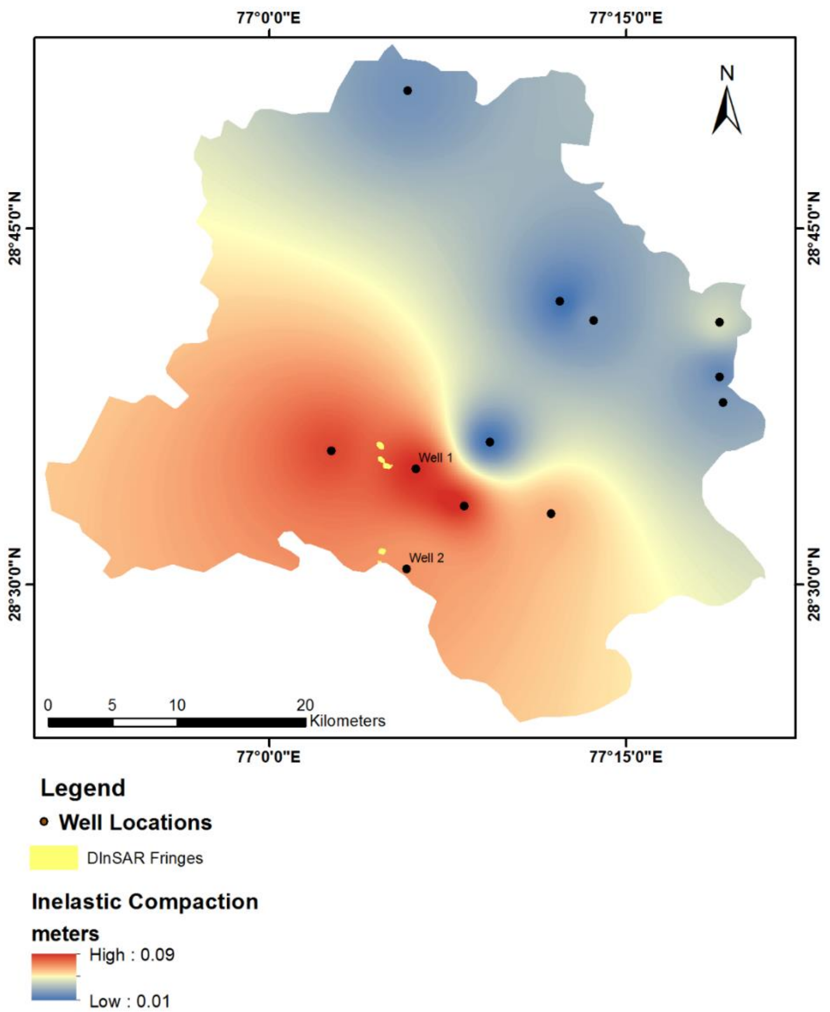

Figure 5.9. Spatial variation of Inelastic Compaction in Delhi

To identify the primary cause of land subsidence, groundwater induced elastic compaction of the aquifer and inelastic compaction of the confining layers were estimated by predictive modelling approach (Table 5.6 and Table 5.7). It was done using piezometric head decline, bulk modulus of compression of aquifer grain structure and confining layers materials, thickness of confining layer and porosity of the aquifer. The land subsidence estimates due to piezometric head decline are 4.5 cm/year (Range: 3.6-6.2) and 2.1(Range: 2.9-4.2) cm/year in Dwarka and Gurgaon respectively (Table 5.8).

The aquifer system compaction rates during 2008-2011 are close to DInSAR measurements which suggests groundwater withdrawal as the primary cause of land subsidence in the area.

6. Conclusion and Recommendation

6.1 Conclusions

In this study an attempt has been made to study the potential of DInSAR technique for identifying probable land subsidence areas. In this work, piezometric data for 2008-2011 has been used to derive aquifer system compaction. 12 wells spread across Delhi were used for the estimation. Decline in piezometric level has shown considerable compaction. Although, elastic compaction of the aquifer is recoverable, the inelastic compaction of the confining layers is irreversible and has serious consequences. This study attempted to find plausible answers to the research questions as follows:

❖ How effectively can DInSAR help in measurement and modelling land subsidence and how can the measurement rates be improved?

Differential Interferograms as obtained from ALOS-1 and RADARSAT-2 show that the highly urbanized parts of Dwarka, Gurgaon & Kharar, Mohali, Banur in Delhi, Chandigarh and surroundings are undergoing land subsidence. In Dwarka, Gurgaon, Kharar, Mohali L-Band (FBS) average deformation rates are 5.7 cm/year, 5.9 cm/year, 5.5 cm/year, and 5.2 m/year respectively during 2009-2011. RADARSAT-2, C-Band average deformation rate in Dwarka (Near Delhi) is 4.5 cm/year over 2013-2015. To improve the measurement rates, coherence based weightage was adopted. InSAR coherence is important in deciding the quality of the interferogram.

❖ How far layer compression is taking place due to groundwater depletion?

Whether groundwater depletion is the cause of land subsidence, predictive modelling was done based on the piezometric head change. Both elastic and inelastic compaction of the aquifer and confining layers have been estimated. The results show potential deformation of 4.5 cm/year and 2.1 cm/year for Dwarka and Gurgaon respectively during 2008-2011. Positive relationship between groundwater depletion and layer compression has been observed.

❖ How far groundwater level decline is correlated with land subsidence and can further help in predicting potential areas?

Land Subsidence areas, as identified by DInSAR, are close to the potentially subsiding areas as identified by predictive modelling. Out of the twelve wells, spread across Delhi, highest compaction was observed in the wells nearby Dwarka and Gurgaon. Therefore, predictive modelling based on piezometry-induced aquifer system compaction can help in identifying potential areas of subsidence.

6.2 Recommendations

Differential fringes tends to appear in every pair at the same geographic location however, atmospheric corrections of the data could be done to get more precise measurement rates.

Precise GPS or levelling measurements in the fringe areas can be used to better quantify land subsidence.

For field validation, extensometer has been installed in Dwarka and the reference measurement has been taken. But, the next observation would be taken just before the onset of monsoons which could be added to the thesis.

References

Abidin, H.Z., Andreas, H., Djaja, R., Darmawan, D., Gamal, M., 2008. Land subsidence characteristics of Jakarta between 1997 and 2005, as estimated using GPS surveys. GPS Solutions 12(1), 23–32. doi:10.1007/s10291-007-0061-0

Amelung, F., Galloway, D.L., Bell, J.W., Zebker, H.A., Laczniak, R.J., 1999. Sensing the ups and downs of Las Vegas: InSAR reveals structural control of lamd subsidence and aquifer-system deformation. Geology. 27(6), 483–486.

Baran, I., Stewart, M.P., Kampes, B.M., Perski, Z., Lilly, P., 2003. A modification to the Goldstein radar interferogram filter. IEEE Transactions on Geoscience and Remote Sensing 41(9), 2114–2118. doi:10.1109/TGRS.2003.817212

Census 2011. Ministry of Home Affairs, Government of India.

Chatterjee, R.S., Fruneau, B., Rudant, J.p., Roy, P.S., Frison, P.L., Lakhera, R.C., Dadhwal, V.K., and Saha, R., 2006. Subsidence of Kolkata (Calcutta) city, India during the 1990s as observed from from space by Differential Synthetic Aperture Radar Interferometry (D-InSAR) technique. Remote Sensing of Environment. 102 (1-2), 176–85. doi:10.1016/j.rse.2006.02.006

Chatterjee, R.S., Syafiudin, M.F., and Abidin, H., 2013. Land Subsidence Characteristics in Bandung City, Indonesia as Revealed by Spaceborne Geodetic Techniques and Hydrogeological Observations. Photogrammetric Engineering and Remote Sensing, 79(7), 639-652.

Chatterjee, R.S., Thapa, S., Singh, K.B., Kumar, G.V., Raju, E.V.R., N.D., 2015. Detection, mapping and monitoring of land subsidence in Jharia Coalfield, Jharkhand, India by spaceborne differential interferometric SAR, GPS and precision leveling techniques.

Ding, X.L., Liu, G.X., Li, Z.W., Li, Z.L., Chen, Y.Q., 2004. Ground subsidence monitoring in Hong Kong with satellite SAR interferometry. Photogrammetric Engineering & Remote Sensing 70(10), 1151–1156.

Domenico, P.A., 1972. Concepts and models in groundwater hydrology. New York: McGraw Hill Book Company. 405.

Fletcher, K., 2007. European Space Agency. European Space Research and Technology Centre. InSAR principles: guidelines for SAR interferometry processing and interpretation. ESA Publications Division, ESTEC, Noordwijk, the Netherlands.

Galloway, D.L., and Sneed, M., 2013. Analysis and simulation of regional subsidence accompanying groundwater abstraction and compaction of susceptible aquifer systems in the USA. Bol. Soc. Geol. Mex 65(1), 123–134.

Galloway, D.L., Hudnut, K.W., Ingebritsen, S.E., Phillips, S.P., Peltzer, G., Rogez, F., and Rosen, P.A., 1998. Detection of aquifer system compaction and land subsidence using interferometric synthetic aperture radar, Antelope Valley, Mojave Desert, California. Water Resources Research 34(10), 2573–2585.

Ganguly, M. 2011. Groundwater withdrawal and land subsidence: A study of Singur Block, West Bengal, India. International Journal of Geomatics and Geosciences 2(2).

Graham, L. C., 1974. Synthetic Interferometer Radar for Topographic Mapping. Proc. of the IEEE, 62(2), 763-768.

Ground Water Year Book 2012-13. Central Ground Water Board, Ministry of Water Resources, Government of India.

Geological and Geomorphological Mapping of Part of NCT Delhi for Seismic Microzonation. Geological Survey of India (GSI), Northern Region.

Haldar, D., Das, A., Yadav, M., Hooda, R.S., Mohan, S., Chakraborty, M., 2014. Analysis of temporal polarization phase difference for major crops in India. Progress in Electromagnetics Research B 57, 299–309.

Hanson, R.T., 1988. Aquifer-system compaction, Tucson Basin and Avra Valley, Arizona.

Helm, D.C., 2003. Techniques for prediction of subsidence, by Germán Figueroa Vega, Soki Yamamoto, and Working Group.

Hoffmann, J., 2003. The application of satellite radar interferometry to the study of land subsidence over developed aquifer systems. Stanford University.

Hsai-Yang Fang and John Daniels., 2006. Introductory Geotechnical Engineering: An Environmental Perspective, Taylor and Francis, 118-120.

Hung, W.-C., Hwang, C., Chang, C.-P., Yen, J.-Y., Liu, C.-H., Yang, W.-H., 2010. Monitoring severe aquifer-system compaction and land subsidence in Taiwan using multiple sensors: Yunlin, the southern Choushui River Alluvial Fan. Environmental Earth Sciences 59, 1535–1548. doi:10.1007/s12665-009-0139-9

Hung, W.-C., Hwang, C., Liou, J.-C., Lin, Y.-S., Yang, H.-L., 2012. Modeling aquifer-system compaction and predicting land subsidence in central Taiwan. Engineering Geology. 147-148, 78–90. doi:10.1016/j.enggeo.2012.07.018

Ichoku, C., Karnieli, A., Arkin, Y., Chorowicz, J., Fleury, T., Rudant, J.P., 1998. Exploring the utility potential of SAR interferometric coherence images. International Journal of Remote Sensing 19(6), 1147–1160.

Jensen, J.R., 2007. Remote Sensing Of the Environment: An Earth Resource Perspective. Pearson Prentice Hall.

Li, Z., Bethel, J., 2008. Image coregistration in SAR interferometry. The International Archives of the Photogrammetry, Remote Sensing and Spatial Information Sciences 37, 433–438.

Lofgren, B.E., 1969. Field measurement of aquifer-system compaction, San Joquin Valley, California, U.S.A. Proc. Tokyo Symp. On Land Subsidence, IASH-UNESCO, 66-79.

Lohman, S.W., 1972. Ground-Water Hydraulics. United States Government Printing Office, Washington.

McCarthy, D.F., 1982. Essentials of Soil Mechanics and Foundations, Reston Publishing Company, Virginia, 632.

Mora, O., Arbiol, R., Palà, V., 2007. ICC's Project for DInSAR Terrain Subsidence monitoring of the Catalonian Territory, in: Geoscience and Remote Sensing Symposium, 2007. IGARSS 2007. IEEE International. IEEE, 4953–4956.

Motagh, M., Djamour, Y., Walter, T.R., Wetzel, H.-U., Zschau, J., and Arabi, S., 2007. Land subsidence in Mashhad Valley, northeast Iran: results from InSAR, levelling and GPS. Geophysical Journal International 168, 518–526. doi:10.1111/j.1365-246X.2006.03246.x

Murthy, V.N.S., 2002. Geotechnical engineering: principles and practices of soil mechanics and foundation engineering. Marcel Dekker Inc., New York.

Ng, A.H., Chang, H., Ge, L., Rizos, C., and Omura, M., 2008. Radar interferometry for ground subsidence monitoring using ALOS PALSAR data, in: Proceedings of The XXI Congress, The International Society for Photogrammetry and Remote Sensing.

Riley, F.S., 1969. Analysis of borehole extensometer data from central California. Land subsidence 2, 423–431.

Rodell, Matthew, Isabella Velicogna, and James S. Famiglietti., 2009. Satellite-Based Estimates of Groundwater Depletion in India. Nature 460 (7258): 999–1002. doi: 10.1038/nature08238.

Rooij, G.H., 2009. Averaging hydraulic head, pressure head, and gravitational head in subsurface hydrology, and implications for averaged fluxes, and hydraulic conductivity. Hydrology and Earth System Sciences 13(7), 1123–1132.

Sahu, P., & Sikdar, P.K., 2011. Threat of land subsidence in and around Kolkata city and East Kolkata Wetlands, West Bengal, India. Journal of earth system science. 120(3), 435–446.

Scheiber, R., & Moreira, A., 2000. Coregistration of interferometric SAR images using spectral diversity. Geoscience and Remote Sensing, IEEE Transactions on 38(5), 2179–2191.

Strozzi, T., Wegmuller, U., Tosi, L., Bitelli, G., Spreckels, V., 2001. Land subsidence monitoring with differential SAR interferometry. Photogrammetric engineering and remote sensing 67(11), 1261–1270.

Todd, D.K., 1980. Groundwater Hydrology. John Wiley and Sons, 45-46.

Venkatramaiah, C., 2006. Geotechnical Engineering. New Age International Publishers Limited, 136-140.

Whittaker B.N., & Reddish, D.V., 1989. Subsidence Occurrence, Prediction and Control. Developments in Geotechnical engineering. 56, 359-360.

Woodhouse, Iain H., 2005. Introduction to Microwave Remote Sensing. CRC Press

Wolkersdorfer, Ch., Thiem G., 2006. Ground water withdrawal and land subsidence in Northeastern Saxony (Germany) Mine Water Environ Association.

Zhou, X., Chang, N.-B., & Li, S., 2009. Applications of SAR Interferometry in Earth and Environmental Science Research. Sensors 9(3), 1876–1912. doi: 10.3390/s90301876

Appendix

ALOS-1 FBS-Dwarka Profiles for the other Years

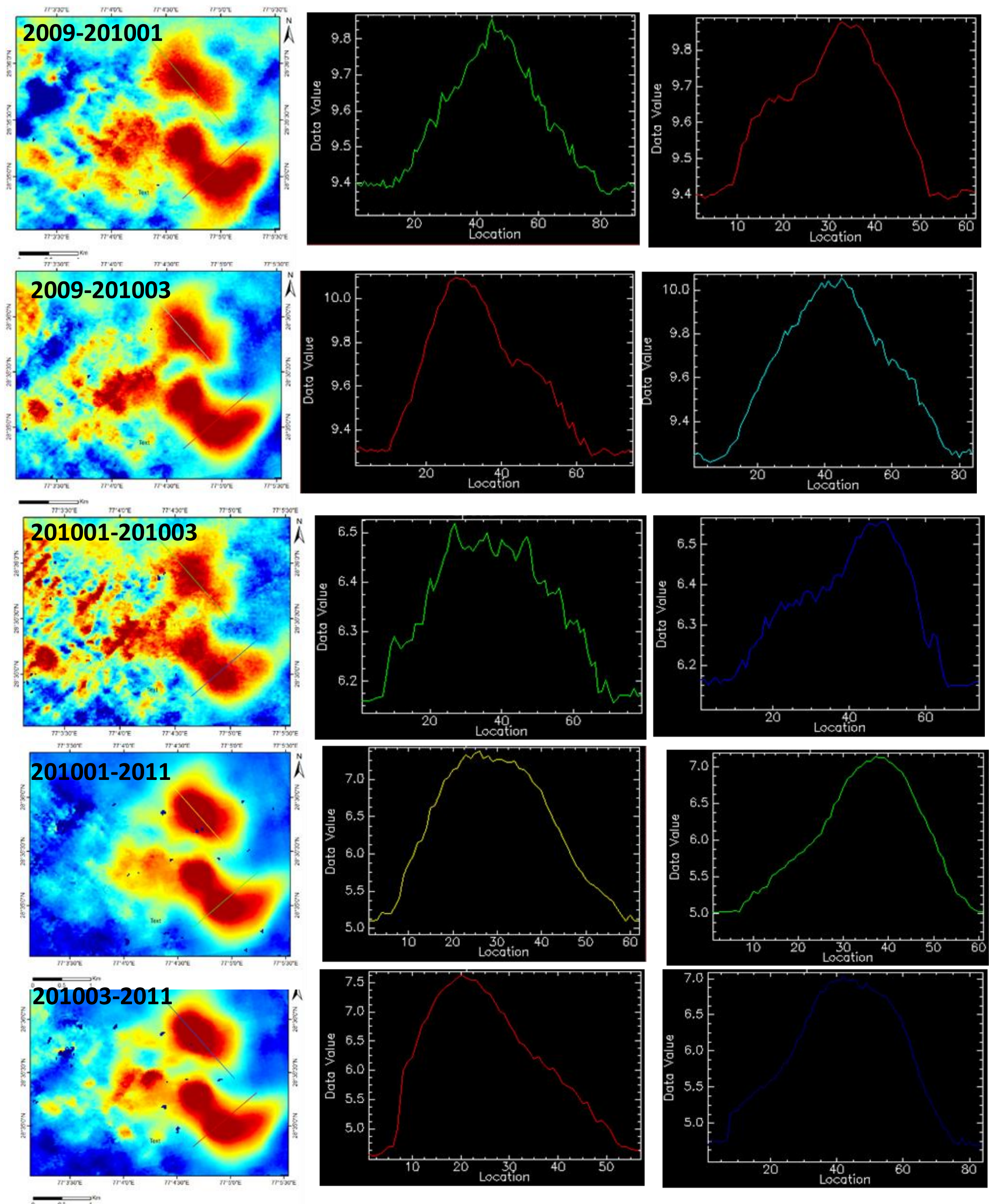

ALOS-1 FBS-Gurgaon Profiles for the other Years

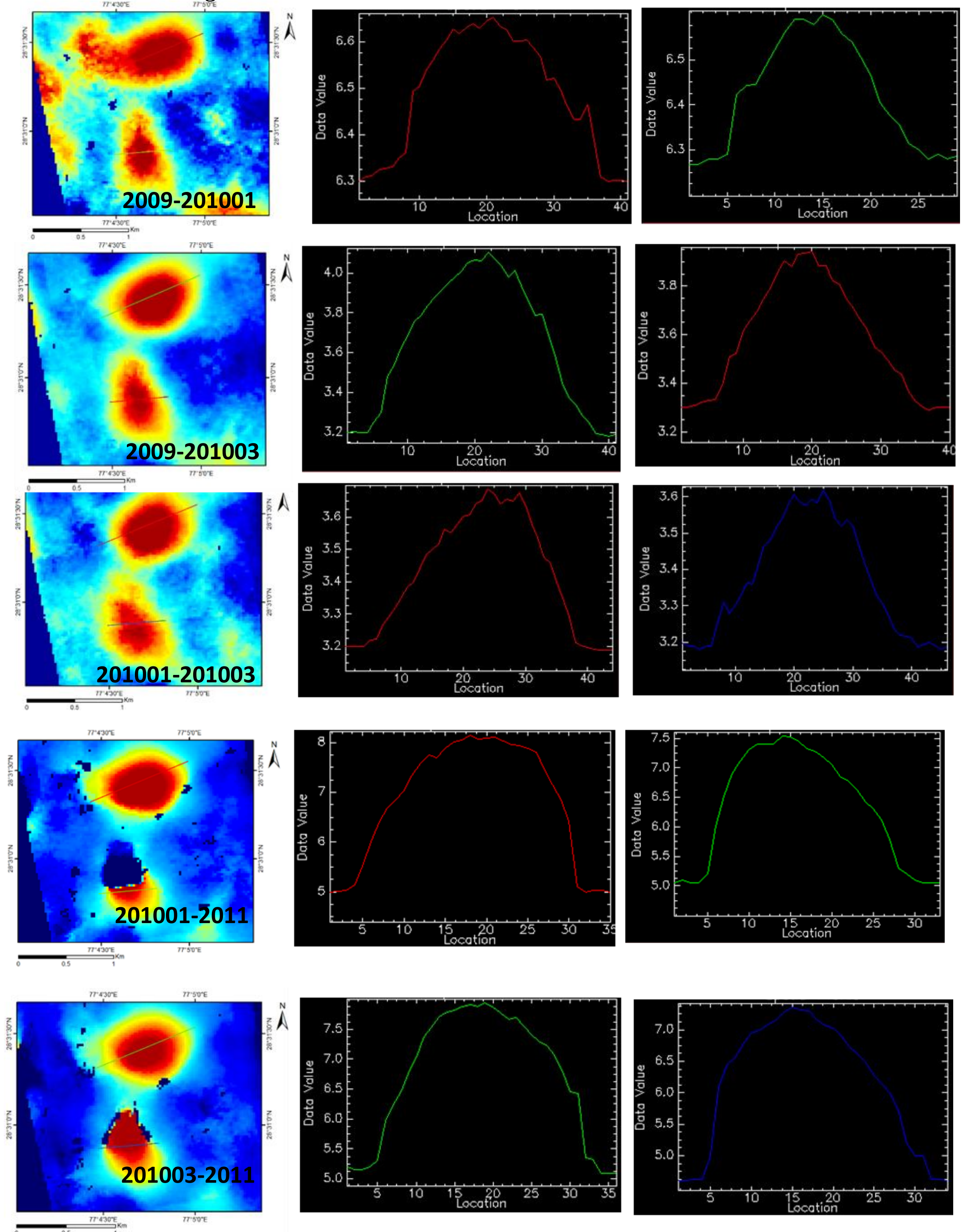

DGPS Survey in Delhi

DGPS Survey in Chandigarh